Journal of Controlled Release 240 (2016) 332–348

Contents lists available at ScienceDirect

Journal of Controlled Release

journal homepage: www.elsevier.com/locate/jconrel

Nanoparticle–liver interactions: Cellular uptake and hepatobiliary elimination

Yi-Nan Zhang [a,b,1], Wilson Poon [a,b,1], Anthony J. Tavares [a,b], Ian D. McGilvray [c,d], Warren C.W. Chan [a,b,e,f,g,*]

[a] Institute of Biomaterials and Biomedical Engineering, University of Toronto, 164 College Street, Toronto, ON M5S 3G9, Canada
[b] Terrence Donnelly Centre for Cellular and Biomolecular Research, University of Toronto, 164 College Street, Toronto, ON M5S 3G9, Canada
[c] Multi Organ Transport Program, Toronto General Research Institute, University Health Network, 200 Elizabeth Street, Toronto, ON M5G 2C4, Canada
[d] Toronto General Research Institute, University Health Network, 585 University Avenue, Toronto, ON M5G 2N2, Canada
[e] Department of Chemistry, University of Toronto, 164 College Street, Toronto, ON M5S 3G9, Canada
[f] Department of Chemical Engineering & Applied Chemistry, University of Toronto, 164 College Street, Toronto, ON M5S 3G9, Canada
[g] Department of Materials Science and Engineering, University of Toronto, 164 College Street, Toronto, ON M5S 3G9, Canada

ARTICLE INFO

Article history:
Received 15 September 2015
Received in revised form 4 January 2016
Accepted 11 January 2016
Available online 13 January 2016

Keywords:
Nanoparticle
Liver
Hepatobiliary clearance
Macrophage

ABSTRACT

30–99% of administered nanoparticles will accumulate and sequester in the liver after administration into the body. This results in reduced delivery to the targeted diseased tissue and potentially leads to increased toxicity at the hepatic cellular level. This review article focuses on the inter- and intra-cellular interaction between nanoparticles and hepatic cells, the elimination mechanism of nanoparticles through the hepatobiliary system, and current strategies to manipulate liver sequestration. The ability to solve the "nanoparticle-liver" interaction is critical to the clinical translation of nanotechnology for diagnosing and treating cancer, diabetes, cardiovascular disorders, and other diseases.

1. Introduction

Nanotechnologies are currently being developed for diagnosing and treating diseases [1–3]. However, most nanoparticles do not reach their intended target and are sequestered by the liver and spleen (if >6 nm) or eliminated though the kidney (if <6 nm) after administration into the body [2,4]. Typically, less than 5% of the injected nanoparticles are delivered to the diseased tissue. The liver acts as a biological filtration system that sequesters 30–99% of administered nanoparticles from the bloodstream. Developing solutions that overcome the liver will be key to enabling the use of nanoparticles for medical applications. This review article is focused on our current understanding of the interaction of nanoparticles with the liver and provides an overview of recent strategies aimed at manipulating liver macrophages to enable longer blood circulation and increase accumulation in the target tissues.

2. Liver anatomy and function

The liver is the largest solid organ in the body. A human adult liver weighs 1.5–2.0 kg on average. The liver is located in the upper right quadrant of the abdomen, below the diaphragm and is partially protected by the rib cage [5]. The structure of the liver consists of two main lobes (Fig. 1). The larger right hepatic lobe and the smaller left hepatic lobe are separated by the course of the middle hepatic vein [5]. The liver is covered by a layer of connective tissue called Glisson's capsule. The main functions of the liver are: (a) production and secretion of bile, (b) storage of iron, vitamins and trace elements, (c) metabolism of carbohydrates and storage of glycogen, (d) volume reservoir and filter for blood, (e) hormonal balance and detoxification, (f) production of immune

Abbreviations: ACO, Aconitylated; ADP, Adenine diphosphate; ATP, Adenine triphosphate; Aco-HSA, Polyaconitylated human serum albumin; Apo, Apolipoprotein; ASGP, Asialoglycoprotein; BSA, Bovine serum albumin; DLPC, Dilinoleoylphosphatidylcholine; DLS, Dynamic light scattering; DOPE, Dioleoylphosphatidyl ethanolamine; DOTAP, 1,2Dioleoyl-3-trimethylammonium-propane; DOX, Doxorubicin; ePC, Egg yolk phosphatidylcholine; EDX, Electron dispersive x-ray; EGF, Epidermal growth factor; FITC, Fluorescein isothiocyanate; Gal, Galactosylated; GA, Glycyrrhetinic acid; GL, Glycyrrhizin; HARE, Hyaluronan receptor for endocytosis; HBVP, Hepatitis B virus preS1-derived lipoprotein; HDL, High-density lipoprotein; HSA, Human serum albumin; HSC, Hepatic stellate cell; ICG, Indocyanine green; ICP–AES, Inductively coupled plasma atomic emission spectroscopy; ICP–MS, Inductively coupled plasma mass spectrometry; ID, Injected dose; INAA, Instrumental neutron activation analysis; LDL, Low-density lipoprotein; LSEC, Liver sinusoidal endothelial cell; M6P, Mannose 6-phosphate; M6P-HSA, Mannose 6-phosphate human serum albumin; MPS, Mononuclear phagocyte system; MRI, Magnetic resonance imaging; MSN, Mesoporous silica nanoparticles; NP, Nanoparticles; PBLG, Poly(γ-benzyl L-glutamate); PEG, Poly(ethylene glycol); PEI, Polyethylenimine; PIC, Polyion complex; PLGA, Poly(lactic-co-glycolic acid); PPAR, Peroxisome proliferator-activated receptor; QD, Quantum dot; RBP, Retinol binding protein; RGD, Arginine-glycine-aspartate; RGDyC, Arg–Gly–Asp–Try–Cys; SPION, Super paramagnetic iron oxide nanoparticle; TEM, Transmission electron microscopy; Tf, Transferrin; TM, Trimyristin.

* Corresponding author at: Institute of Biomaterials and Biomedical Engineering, University of Toronto, 164 College Street, Toronto, ON M5S 3G9, Canada.
E-mail address: warren.chan@utoronto.ca (W.C.W. Chan).

[1] These authors contributed equally to this work.

http://dx.doi.org/10.1016/j.jconrel.2016.01.020
0168-3659/

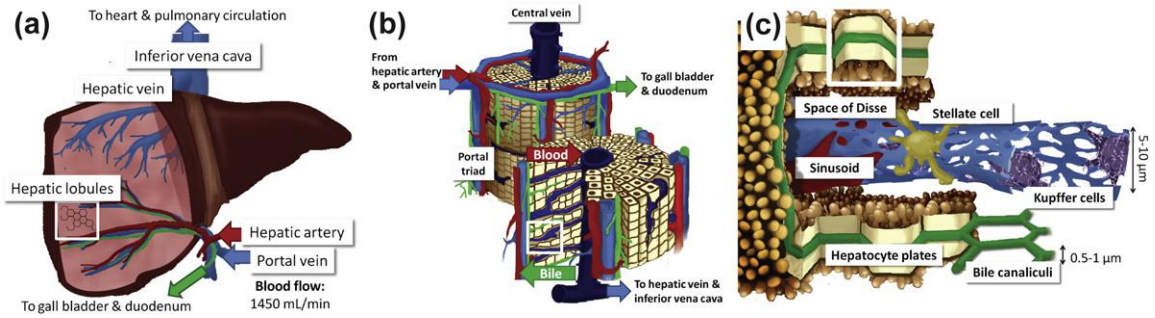

Fig. 1. Structure of the liver. (a) The hepatic artery and portal vein supply the blood, nutrients and oxygen to the liver. The gallbladder collects and stores the bile. (b) The liver lobules. The liver parenchyma consists of hexagonal lobules, including hepatocyte plates and sinusoids. Portal triads are at the corners of the lobules and contain the hepatic artery, portal vein, and bile duct. The blood flows in through the portal vein and hepatic arteries, then flows out through the hepatic vein and inferior vena cava. (c) The liver sinusoid. Blood flows from both the hepatic artery and portal vein and mixes in hepatic sinusoids. Reprinted with permission from [11]. Copyright 2012 Elsevier.

factors to fight infection against pathogens, and (g) conversion of waste products for excretion by the kidneys and intestines [6-9].

The liver is a complex network of inter-related cells (Fig. 1). About 60–80% of parenchymal cells are hepatocytes, which are specialized epithelial cells [10]. Additional cells include Kupffer cells and motile macrophages, liver sinusoidal endothelial cells (LSECs), hepatic stellate cells (HSCs), biliary epithelial cells (cholangiocytes), resident immune cells (dendritic cells, natural killer cells and lymphocytes) and circulating blood cells that are in transit through the liver [10]. Kupffer cells make up 80–90% of the total body macrophage population [9] and are responsible for the majority of phagocytic activity in the liver [11]. LSECs form the continuous lining of liver capillaries and create sinusoidal fenestrations where HSCs can be activated and respond to liver damage [12–14].

The liver has two major sources of blood supply: the hepatic artery and portal vein [5,15]. The left and right hepatic arteries supply the liver with oxygen-rich blood from the heart. This accounts for only 25–30% of the blood to the liver, but 70% of the oxygen. The portal vein carries nutrient-rich (but relatively less oxygenated)– blood from the spleen, pancreas and intestines to the liver and constitutes the remaining 65–70% of blood volume. Hepatic arterial and portal blood combine in hepatic sinusoids. The majority of the blood is then drained from the liver through the left, middle and right hepatic veins [14].

The liver can be conceptualized as being organized into hexagonal prism-shaped portal and hepatic lobules [5]. The central vein (hepatic vein) is located in the center of each lobule, ultimately draining into a larger hepatic vein and subsequently to the inferior vena cava for transport back to the heart as shown in Fig. 1b [14]. Central veins are connected to the portal triads through liver sinusoids. Portal triads are at the corners between adjacent lobules. Each portal area consists of the hepatic artery, portal vein, and bile duct, that facilitate the transport of oxygen, nutrients and bile, respectively [7].

The blood from both the hepatic artery and portal vein mixes together in hepatic sinusoids before the blood drains out of the liver to the heart through the central vein [5,14] (Fig. 1c). Sinusoids contain a variety of liver cells including resident tissue macrophages, Kupffer cells, that can remove synthetic particles from circulation [16]. Endothelial cells line liver sinusoids and form fenestrae. These fenestrations allow blood plasma to interact with the hepatocytes through the space of Disse, a small region between the endothelial and hepatocyte layers. Plasma contains many types of enzymes (such as glycogen synthase) [17] that enable the breakdown and metabolism of various biomolecules (such as cholesterol, and bilirubin) in bile ducts. In addition, HSCs are another class of cells located in the liver [9]. They are specifically located within the space of Disse and are responsible for responding to liver injury and assisting in tissue repair.

Finally, the liver, gallbladder and small intestine are connected to the liver by the intrahepatic and extrahepatic biliary tree. The trunk of the tree is formed by the confluence of the right and left bile ducts, draining the right and left lobes of the liver. The branches are formed by progressively smaller ducts draining the liver parenchyma. Within the parenchyma, bile is formed in hepatocytes and then exported into the canaliculi that run between hepatocytes and drain into the ducts of the portal triads. Hepatocytes produce bile for food digestion and for the elimination of biological waste. Bile will travel through and along the intrahepatic biliary tree from the liver to the duodenum (the first part of the small intestine) or to the gallbladder for temporary storage. The gallbladder is a small sac-shaped organ that stores and concentrates bile. A large number of stimuli, including the passage of food into the intestine, will cause the bile to be excreted from the gallbladder and biliary tree into the intestine.

3. The interaction of nanoparticles with hepatic cells

The interactions of engineered nanoparticles with liver cells determine the fate of administered nanoparticles in vivo. However, how the specific or combination of nanoparticle physicochemical properties determines their liver sequestration and cell interaction in vivo remain unknown. In vivo studies are mostly focused on the accumulation of the nanoparticles at the organ level, while most in vitro studies are focused on a single hepatic cell type in culture and do not consider how the unique architecture and position of cells within the liver affect their interaction. It is known that most nanoparticles are typically taken up by non-parenchymal cells despite the majority of cells in the liver being comprised of parenchymal hepatocytes. Particles that interact with hepatocytes can be cleared from the body via the hepatobiliary pathway. This section discusses nanoparticle uptake by liver cells. The specific ligand–receptor interactions involved in phagocytosis are summarized along with physicochemical properties of nanoparticles in Table 1 for non-parenchymal cells and Table 2 for parenchymal cells of the liver.

3.1. Kupffer cells

Kupffer cells are positioned in liver sinusoids and are an important first line of innate immunity. Kupffer cells are tissue resident macrophages that phagocytose and destroy pathogens and other foreign bodies and materials in the blood. These macrophages are also involved in the recycling of erythrocytes and the digestion of apoptotic cells. Circulating monocytes in the blood adhere to liver tissue and are polarized into Kupffer cells with highly differentiated surface receptors that facilitate the binding and/or uptake of foreign materials [18,19]. The rate of uptake and retention in the cells is strongly correlated with the nanoparticle's surface charge, ligand chemistry and size. Nanoparticles with highly cationic and anionic surface charges adsorb a significant amount of serum proteins to form a 'protein corona', may aggregate, and display an increased interaction with macrophages in vitro [20]. The majority of neutral surface ligands for nanomaterials are based on coating with poly(ethylene glycol) (PEG). Fewer serum proteins adsorb to the PEG surface of nanoparticles than cationic or anionic surfaces, and

Table 1
Nanoparticle formulations organized by non-parenchymal cell type, nanoparticle physicochemical properties and the ligand-receptor interaction for selective association.

Cell type	Receptor–ligand system		Nanoparticle characteristics			Cell line/animal model	Reference
	Receptor	Ligand	Core type	Size	Zeta potential		
Kupffer	Galactose	Lactobionic acid	LDL	27 nm	n/a	ANA1, primary peritoneal macrophages and HSCs from C57BL/6-J mice, & C57BL/6-Tg-Thy1.1 mice	[39]
	Mannose	Mannose-BSA	Liposome	~95 nm	n/a	Male ddY and CDF1 mice	[40]
				64.6 ± 1.70 nm	+61.4 ± 0.91 mV	Female ICR mice, female C57BL/6 mice	[41]
	Scavenger	BSA	QDs	34.6 nm	−29.7 mV	Primary Kupffer from Sprague-Dawley rats	[21]
Endothelial/Kupffer	Scavenger	Poly-Aco-HAS	Liposome	92.1, 153.5, 263.2, and 590.7 nm	n/a	WAG/Rij rats	[27]
Endothelial	Low-density lipoprotein LDL	KLGR peptide	Polycation-encapsulated plasmid coated with lipid bilayer	84–118 nm	+6.1 mV to +25.7 mV	Primary ICR mice liver sinusoid endothelial cells, Hepa1–6 & ICR mice	[42]
	HARE	Hyaluronic acid	Plasmid-PEI micelle	20–22 nm	−1.8 mV to −4.6 mV	C57BL/6 mice, exon 16-knockout hemophilia A mice	[43]
Endothelial/stellate	HARE CD44, IFNα	Hyaluronan acid, IFNα	Gold	52.23 nm	n/a	BALB/c mice	[44]
Stellate	Collagen type VI	cRGD peptide	Liposome	101 ± 17.7 nm	n/a	HSCs isolated from the Male Wistar rats in vitro. Male Wistar rats in vivo	[31]
	Mannose	mannose	Liposome	50–400 nm	n/a	C57BL/6 mice	[45]
	6-phosphate/insulin-like growth factor 2	6-phosphate -HSA	Mannose-6-phosphate-modified BSA	122.7–262.8 nm	−2.73 mV to −35.85 mV	Kunming mice, SD rats	[46]
			Liposome	92.37 ± 3.28 nm	−19.7 ± 1.72 mV	Sprague–Dawley rats	[47]
			DLPC-liposome	81 ± 11 nm	n/a	HSCs isolated from Wistar rats, bile duct ligated Wistar rats	[48]
	Platelet-derived growth factor receptor β	Cyclic (SRNLIDC) peptide	Sterically stable liposome	86.9 nm	n/a	Primary SD rat HSCs, TAA-induced fibrotic SD rats	[49]
	RBP	Retinol (vitamin A)	Hyaluronic acid–cystamine–glycyrrhetinic acid	383 nm	+15.5 mV	Primary ICR mouse HSCs, hepatic stellate cell-T6, BDL liver fibrosis model ICR mice	[50]
			POEGMA-b-VDM diblock copolymer	35 nm	n/a	LX-2, SD rat	[32]
			Liposome	296.2 ± 32 nm	n/a	LI90 cells (human HS cell line), dimethylnitrosamine (DMN) treated Male Sprague–Dawley rats	[51]
			Retinol-polyetherimine	383 nm	+15.5 mV	Primary ICR mouse HSCs, hepatic stellate cell-T6, BDL liver fibrosis model ICR mice	[52]
	$\alpha_v\beta_3$ integrin	Cyclic (RGDyC) peptide	Superparamagnetic iron oxide	13 nm	n/a	Hepatic stellate cell-T6 & SD rats	[53]

Table 2
Nanoparticle formulations organized by parenchymal cell type, nanoparticle physicochemical properties and the ligand-receptor interaction for selective association.

Cell type	Receptor–ligand system		Nanoparticle characteristics			Cell line/animal model	Reference
	Receptor	Ligand	Core type	Size	Zeta potential		
Hepatocyte/hepatoma cell	ASGP	Lactobionic acid	Superparamagnetic iron oxide	26 nm	n/a	Hepatocytes isolated from a SD rat, rabbits	[54]
				12 nm	n/a	HepG2 human hepatocyte carcinoma cell line, BALB/c mice	[55]
			Silica	60 nm	+16 mV	BEL-7404	[56]
			TM, ePC, Gal-DOPE Solid lipid	120.4 ± 10.4 nm	−12.4 ± 1.1 mV	BEL-7402 cell in vitro, C57BL/6 mice and female nude mice	[57]
		Lactobiotin	Stearic acid grafted chitosan micelles	~100–120 nm	+27.8 mV	HepG2, BEL-7402 & HepG2 tumor-bearing nude mice	[58]
		Lactose	PIC micelles	49.5 ± 0.6 nm (by DLS), 26.4 ± 4.0 nm (by TEM)	+17.16 ± 4.38 mV	Male Sprague–Dawley rats	[59]
		Galactosyl	Polyphosphate	130 nm	−18.4 mV	HepG2, Male Wistar rats	[60]
		Galactose	Liposomes	195 ± 17 nm	−10.6 ± 1.2 mV	HepG2, KM mice	[61]
				138.03 ± 1.10 nm	+56.50 ± 1.08 mV	Hepatocytes, CD-1 mice	[62]
				115.9 ± 0.46 nm	+14.17 ± 1.38 mV	C57BL/6 mice	[63]
			PLGA	198.1 ± 1.2 nm	−8.5 ± 1.5 mV	BALB/c mice	[64]
			Polystyrene	50 nm	n/a	Primary BALB/c mouse hepatocytes & BALB/c mice	[28]
			Galactoylated chitosan	35.19 ± 9.50 nm	+10.34 ± 1.43 mV	SMMC-7721, SW480 and LO2 cell lines, H22 orthotopic liver cancer mice	[65]
				282.2 ± 15.3 nm	−12.88 ± 1.72 mV	Sprague–Dawley rats and Kunming strain mice	[66]
		Galactosamine	Poly(γ-glutamic acid)-poly(lactide)	115–263 nm	−23 to −19 mV	HepG2	[67]
				127.5 nm	−10.6 mV	HepG2 & HepG2 tumor-bearing BALB/c mice	[68]
		Galactoside	Galactosylated liposome	~79 nm	n/a	Female KM mice	[69]
		Pullulan	Polyethylene sebacate	103–335 nm	−18 to −25 mV	Sprague–Dawley rats	[70]
		Soybean sterylglucoside	Liposomes	96.2 nm, and 183.0 nm	+	HepG2, Male KM mice	[71]
		Asialoorosomucoid	Plasmid-PEI micelle	21–29 nm	−0.8 mV to −8.6 mV	C57BL/6 mice, exon 16-knockout hemophilia A mice	[43]
	Glycyrrhetinic acid/glycyrrhizin receptor	Glycyrrhetinic acid/glycyrrhizin	Recombinant HSA	170 nm	~ −25 mV	HepG2 & H22 tumor-bearing BALB/c nude mice	[35]
			Chitosan	188.8–231.6 nm	+12.71 mV to +36.55 mV	QGY-7703, H22 tumor-bearing CD1 nude mice, & Wistar rats	[36]
				147.2 nm	+9.3 mV	Primary Wistar rat hepatocytes	[38]
				217.2 nm	+30.6 mV	SMMC-7721, LO2, and SW480 cell lines, H22 orthotopic tumor-bearing mice	[72]
				164.5–183.4 nm	−30.7 to −26.9 mV	HepG2 cells, Kunming mice	[73]
				112–203 nm	−31 to −28 mV	SMMC-7721 cells, H22 tumor-bearing mice	[74]
			PEG-PBLG micelles	181.8 nm	n/a	7703 cells, Wistar rats	[75]
			Alginate	274.2 nm	−45.6 ± 2.3 mV	HepG2, H22 tumor-bearing Kunming mice	[76]
				241.2 ± 9.5 nm	−43.1 ± 1.24 mV	HepG2, H22 tumor-bearing Kunming mice	[77]
	PPAR	Linoleic acid	Superparamagnetic iron oxide-chitosan	95.3 nm	+49.8 mV	Primary BALB/c mice hepatocytes & BALB/c mice	[78]
	Heparan sulfate glycosaminoglycan	CKNEKKNKIERNNKLKQPP-peptide	Liposome	120.8 nm	0 mV to +8.8 mV	BALB/c mice	[79]
	CXC receptor type 4	AMD3100	DOPA-PLGA	175.25 nm	−19 mV	HCA-1, JHH-7, & HCA-1 tumor-bearing orthotopic C3H/HeNCrNarl mice	[80]
	HARE, glycyrrhetinic acid receptor	Cleavable hyaluronic acid-glycyrrhetinic acid	Cleavable hyaluronic acid-glycyrrhetinic acid	190.9 nm	−21.93 mV	HepG2 cells, H22 tumor-bearing Kunming mice, HepG2 tumor-bearing athymic nude mice	[50]
	HBVP receptor	Hepatitis B virus preS1-derived lipoprotein	PEGylated Liposome	150 nm	−14.5 mV to −16.8 mV	Primary ICR mice hepatocytes & ICR mice	[81]
	HDL	Apo-AI	Gadolinium	20–25 nm	−30.2 to −59.7 mV	HepG2 & SD rats	[82]
			Iron oxide	7–13 nm	n/a	HepG2 & ApoE knockout mice	[83]
	Scavenger receptor class B member 1		DOTAP/cholesterol	148–177 nm	+39 to −50 mV	HepG2, nude mice, C57BL/6 mice, BALB/c mice	[84]
	LDL	LDL	Gold	20 nm	n/a	SD rats	[85]

PEGylated nanoparticles are taken up less efficiently by phagocytic cells than more charged nanoparticles. For example, the interaction between quantum dots (QDs) and primary Kupffer cells was studied by Fischer et al. [21]. QDs functionalized with PEG demonstrated reduced uptake compared to those coated with bovine serum albumin (BSA), where the latter was completely internalized within 60 min after administration. Kupffer cells also show increased phagocytosis of nanoparticles with larger diameters. The uptake of 90 nm gold nanoparticles was increased by four times compared to those one third in size of identical surface composition using J774A.1 macrophages in vitro [20].

Kupffer cells recognize nanoparticles as a foreign material and the nanoparticles can be internalized through multiple scavenger receptors. They will be taken up by the mechanisms of macropinocytosis, clathrin-mediated, caveolin-mediated endocytosis, and additional endocytotic pathways [22]. Studies that elucidate uptake mechanisms are highlighted in a study by Lunov et al. that evaluated the uptake of 20 nm and 60 nm superparamagnetic iron oxide nanoparticles (SPIONs) by human macrophages [23]. Carboxy-dextran coated SPIONs were found to accumulate in macrophages through clathrin-mediated and scavenger receptor A endocytosis irrespective of size. 60 nm SPIONs displayed sixty-fold higher uptake than 20 nm SPIONs. This pathway was confirmed by preparation of knockout macrophages and through the use of rottlerin, colchicine, cytochalasin B, monodansyl cadaverine, and nystatin as selective inhibitors of micropinocytosis, pinocytosis, phagocytosis, clathrin-mediated, and calveolin-mediated endocytosis, respectively. Uptake of SPIONs was reduced by more than 80% in the presence of clathrin-mediated and scavenger receptor A endocytotic inhibitors. Furthermore, a reduction of SPION uptake in the presence of rottlerin was also reported, suggesting that macropinocytosis may also contribute to internalization. In the same study, theoretical modeling of the endocytosis pathways suggested that 2 to 20 receptors are involved in the endocytosis of SPIONs [23]. Larger nanoparticles may display increased avidity due to their greater surface area for interaction with the cell membrane and adjacent receptors.

For many applications of nanotherapeutics, the interaction and removal of nanoparticles from the bloodstream by Kupffer cells are regarded as a significant challenge to targeting of diseased tissues for diagnosis or therapeutic applications. Within the last few years, methods have been developed to delay, prevent, or remove this interaction in an effort to improve the transport of nanoparticles to the desired diseased tissue. These strategies are described in detail in Section 5. Perhaps one opportunity in targeting nanoparticles to Kupffer cells may be for treatment of autoimmune disorders. During an immune response, Kupffer cells release a high degree of pro-inflammatory markers and cytokines and may aggravate tissue inflammation. In the case of cirrhosis, transient depletion of Kupffer cells led to an improvement in liver inflammation [24]. Since any injected formulation of nanoparticles will ultimately be sequestered by Kupffer cells, they may be well suited as a carrier to suppress or eliminate a pro-inflammatory response.

3.2. Sinusoidal endothelial cells

Sinusoidal endothelial cells form a continuous lining along the vasculature of the sinusoid. LSECs are highly pinocytic, relying on scavenger receptors to remove materials from the bloodstream, and are also involved in innate immunity [25]. LSECs lack the typical basement membrane common to the endothelial cells of other tissues and contain fenestrae with pore sizes ranging from 100 to 150 nm [25]. As nanoparticles enter the sinusoid, interactions with endothelial cells may occur. LSECs are involved in the removal of waste macromolecules like hyaluronan, connective tissue components and materials from circulation in the blood through receptor–ligand interactions [26]. Some major receptors involved include mannose, Fcγ, collagen-alpha receptor, and the hyaluronan scavenger receptors. It is worth highlighting that the former two surface receptors are also expressed by Kupffer cells. It is highly plausible that both cell types compete for nanoparticles in circulation through the sinusoid [26]. Additionally, the mechanism of cellular internalization is dependent on the physicochemical properties of the nanoparticle such as the hydrodynamic size. For example, nanoparticles that are over 100 nm in diameter or sub-100 nm that are aggregated would have higher interaction with Kupffer cells. In contrast, smaller monodisperse nanomaterials may be taken up by LSECs to a higher degree. The specific mechanism of interaction and uptake may be due to a combination of physicochemical properties (e.g., size and the type of serum proteins adsorbed). Some insights into this hepatic cellular distribution were reported by investigating the targeting of LSECs with polyaconitylated human serum albumin (Aco-HSA) liposomes [27]. It was found that 80% of the injected Aco-HSA liposomes accumulated in hepatic tissues 30 min after intravenous injection. In reference to control liposomes, a 17-fold increase in the liver was noted with Aco-HSA liposomes. Of the total amount of nanoparticles in hepatic tissues, two-thirds of the Aco-HSA liposomes were taken up by LSECs, while the others were sequestered by Kupffer cells. As the size of Aco-HSA liposomes were increased from 50 to 400 nm, the uptake by LSECs decreased by a factor of approximately three with a correlated increase in uptake by Kupffer cells. On a related note, in a study investigating the hepatic tissue distribution of 50 and 140 nm polystyrene beads terminated with galactose and methoxy functional groups, the majority of the administered nanoparticles accumulated in Kupffer cells and hepatocytes. Electron microscopy and flow cytometry data demonstrated no interaction and uptake by LSECs or HSCs [28]. At present, there are only limited numbers of investigations that focus on understanding the hepatic distribution of nanoparticles at a cellular resolution across a plethora of nanoparticle physicochemical properties. Despite some evidence to support the ability of LSECs to take up nanoparticles, the current general consensus within the nanotechnology field is that nanoparticles are predominantly sequestered by macrophages.

3.3. Hepatic stellate cells

Stellate cells are involved with the secretion and maintenance of extracellular matrix. They contain a large reservoir of vitamin A in the liver and respond to damaged hepatocytes and immune cells by differentiating into tissue-regenerating myofibroblasts [29]. HSC-targeting nanoparticles may have implications on the treatment of liver fibrosis. A series of surface receptors can be targeted to direct nanoparticles toward these cells in hepatic tissues if they are not first removed from circulation by Kupffer cells and LSECs. These surface receptors include: mannose 6-phosphate (M6P)/insulin-like growth factor-II receptor, type VI collagen and integrins, and retinol binding protein (RBP) [14]. Cyclic peptides containing the arginine–glycine–aspartate (RGD) motif can bind to the collagen type VI receptors on HSCs and offer a selective nanoparticle interaction. For example, Beljaars et al. [30] reported that human serum albumin conjugated with these peptides (CVI-HSA) can be taken up by HSCs. RGD-labeled liposomes showed ten times higher accumulation in HSCs than liposomes without RGD peptide [31]. A similar study by Duong et al. [32] demonstrated that diblock co-polymer nanoparticles loaded with S-nitrosoglutathione and coated with vitamin A can increase uptake via RBP by HSCs 30% more than nanoparticles without vitamin A. HSCs comprise less than 10% of the total amount of cells in the liver and reside in the space of Disse adjacent to endothelial cells [29]. This anatomical location provides a challenge for distributing nanoparticles to these cells and it is more than likely a majority of nanoparticles will be internalized by Kupffer cells and LSECs prior to interaction with stellate cells.

3.4. Hepatocytes and hepatocellular carcinoma cells

A basic understanding of how to target hepatocytes may be critical to eliminating nanoparticles through the hepatobiliary route. There are several strategies to design nanoparticles to access and

interact with hepatocytes: (1) sinusoidal intercellular junctions and (2) transcytosis through the sinusoidal endothelial cell lining. Hepatocytes constitute 70–80% of the cells in the liver and are involved in the maintenance of liver functions. A wide variety of nanoparticles have been designed to target these cells [14]. The most commonly targeted receptors used to direct nanoparticles to hepatocytes and hepatocellular carcinoma cells, include: asialoglycoprotein (ASGP) receptor, glycyrrhizin/glycyrrhetinic acid receptor, transferrin (Tf) receptor, low-density lipoprotein (LDL) receptor, high-density lipoprotein (HDL) receptor, hyaluronan receptor for endocytosis (HARE), and immunoglobulin A binding protein [9,13,33]. ASGP is the most well-characterized hepatocyte-specific receptor system [33]. One of the main advantages of using this ASGP receptor is its innate binding affinity to a wide range of molecules containing galactose and N-acetyl-galactosamine residues, such as lactose, lactobionic acid, galactoside, galactosamine and asialofetuin. Glycyrrhizin/glycyrrhetinic acid (GL/GA) receptors are expressed on the membrane of hepatocytes as well as other cell types in the kidneys, stomach, and colon to take up glycyrrhizin/glycyrrhetinic acid via receptor-mediated endocytosis [34–37]. While GL/GA receptors are not as specific to hepatocytes as ASGP receptors, their corresponding ligands GL and GA have anti-hepatitis and anti-hepatotoxic functionality [37], marking them useful for actively targeting nanoparticles to hepatic diseases. The interaction between polymeric chitosan nanoparticles surface-modified with glycyrrhizin (CS-GL nanoparticles) and hepatocytes was studied using flow cytometry and confocal laser microscopy [38]. The result showed that CS-GL nanoparticles preferred to be taken up by hepatocytes and the uptake amount was almost five times higher than hepatic non-parenchymal cells. In vivo studies show that both doxorubicin (DOX) loaded and glycyrrhetinic acid modified recombinant human serum albumin nanoparticles (DOX/GA-rHSA nanoparticles) [35] and DOX-loaded chitosan/poly(ethylene glycol)-glycyrrhetinic acid (CTS/PEG-GA) nanoparticles [36] can effectively inhibit tumor growth in H22 tumor-bearing mice. Other clinically relevant hepatocyte and hepatocellular carcinoma ligand-receptor systems include Tf and LDL systems due to their efficient receptor recycling, enabling more rounds of endocytosis before receptor desensitization or down-regulation [33].

4. Hepatobiliary clearance of nanoparticles

Since the metabolism and clearance of foreign materials are major functions of the liver, engineered nanomaterials that cannot be cleared by the renal system will eventually be processed in the liver. The general scheme for nanoparticle clearance is through three main mechanisms: renal, hepatobiliary, and via the mononuclear phagocyte system (MPS) as outlined in Fig. 2 [4,86].

4.1. Nanoparticle transport through the hepatobiliary system

In hepatobiliary clearance, hepatocytes in the liver eliminate foreign substances and particulates by endocytosis, followed by their enzymatic breakdown and excretion into the bile via the biliary system [87]. This process is schematically shown at the organ and tissue level in Fig. 3. Nanoparticles enter the liver via portal triads. To successfully transit through the biliary system, nanoparticles must first avoid becoming sequestered in Kupffer cells. Kupffer cells have been shown to take up nanoparticles on a broad size scale spanning several hundreds of nanometers [88,89]. Circulating nanoparticles smaller than the diameter of liver sinusoidal fenestrations (up to 150–200 nm) can extravasate into the space of Disse and interact directly with hepatocytes [9,25,90,91]. Aside from this transport, interaction with LSECs and transcytosis to underlying hepatocytes may be an alternate pathway to afford nanoparticle–hepatocyte interaction. The nanoparticle surface charge has also been shown to alter uptake by hepatic cell types due to differences in nanoparticle–cell membrane electrostatic interactions and protein adsorption to the nanoparticle surface [44,58]. As described previously, LSECs and Kupffer cells abundantly express scavenger receptors on their surfaces that are efficient at binding to negatively-charged nanoparticles [9,92,93]. On the other hand, hepatocytes were found to take up positively-charged nanoparticles but not their negatively-charged counterparts [9,92].

In Fig. 4 and Table 3, the hepatobiliary clearance efficiency, which is loosely defined as the percentage of injected dose of nanoparticles excreted in feces following intravenous administration, is compiled as reported from the literature for a wide variety of nanoparticle designs

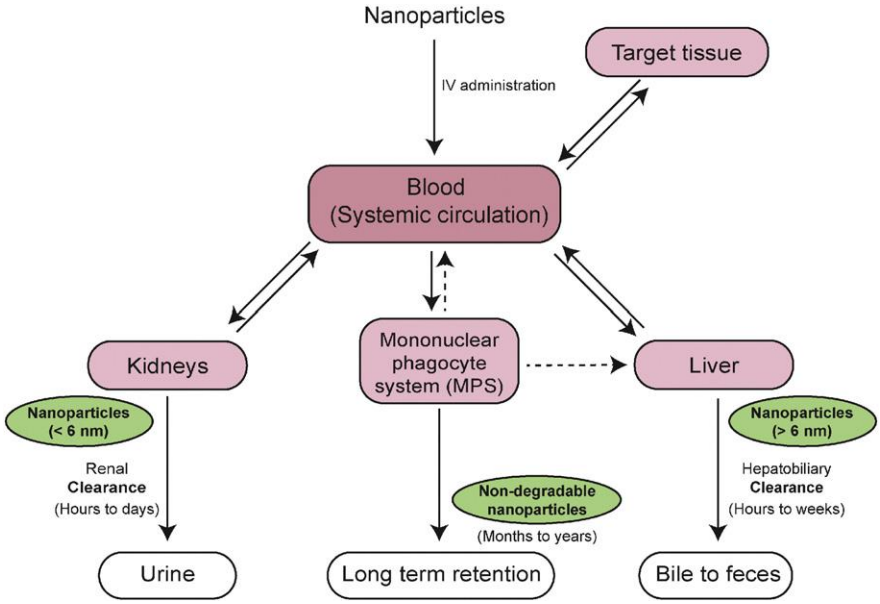

Fig. 2. Schematic of nanoparticle clearance pathways. Nanoparticles are cleared through hepatobiliary, renal, and mononuclear phagocyte systems. Solid arrows indicate the most probable interaction, dashed arrows indicate possible interaction. Nanoparticles circulate in the blood to reach diseased tissue. If nanoparticles are less than 6 nm in size, they can be cleared from the kidney by renal clearance within hours to days after administration. Larger-sized non-degradable nanoparticles are more likely to be taken up and retained by the MPS. If nanoparticles are degradable by the MPS, their substituents may escape sequestration and return to blood circulation for eventual hepatobiliary or renal clearance. Of note, the MPS includes phagocytes in the liver. Adapted with permission from [4]. Copyright 2015 American Chemical Society.

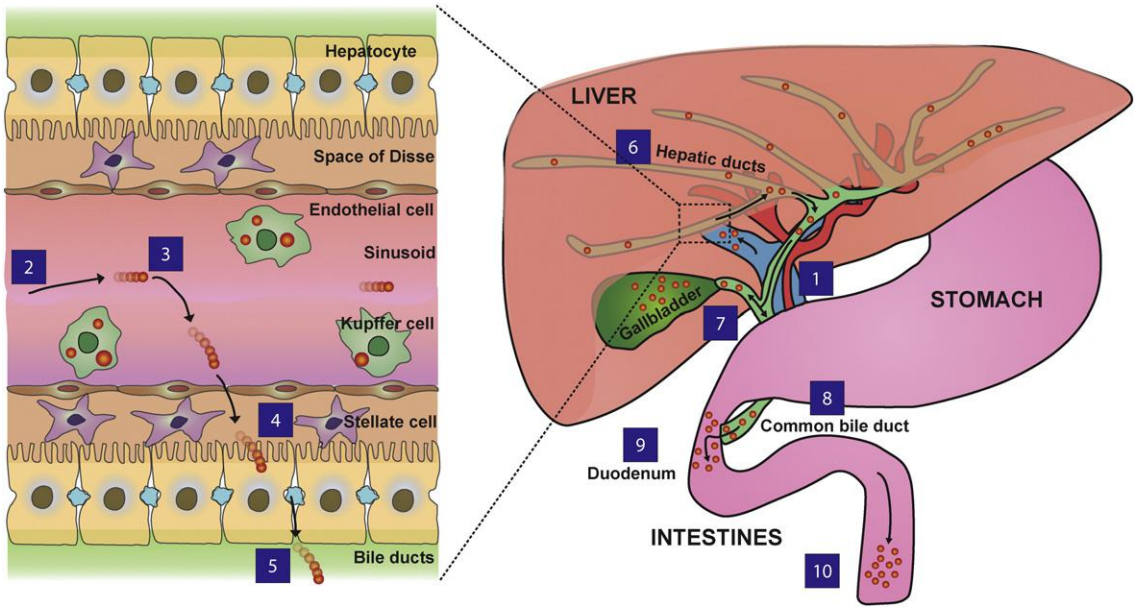

Fig. 3. Schematic of the hepatobiliary processing and clearance of nanoparticles. (1) Nanoparticles enter the liver via the portal vein. (2) Nanoparticles traverse the hepatic sinusoid and (3) may be taken up and sequestered in liver resident Kupffer cells. (4) Depending on their physicochemical properties, nanoparticles may filter out into the space of Disse and be endocytosed by hepatocytes. (5) Nanoparticles transcytose through the hepatocytes and enter the bile duct via bile canaliculi. (6) Nanoparticles travel through the hepatic ducts. (7) Depending on digestive state and bile production, nanoparticles may first collect inside the gallbladder or (8) nanoparticles may enter into the common bile duct. (9) Nanoparticles are excreted into the duodenum of the small intestines via the sphincter of Oddi. (10) Nanoparticles eventually traverse the entire gastrointestinal tract and are eliminated in feces.

[4,85,94–103]. The physicochemical properties of nanoparticles, including core type, surface chemistry, size, shape, and surface charge, dictate their interaction with hepatocytes and are responsible for the wide discrepancy in hepatobiliary clearance seen across variable nanoparticle designs. This data supports the notion that hepatic processing and biliary excretion is usually slow, ranging from hours to months or longer [87,104]. The prolonged retention of nanoparticles from this relatively slow clearance pathway and associated complex catabolites raises the concern of chronic toxicity to the liver parenchyma [87,105]. Hematology indicators such as the total red blood cell count, hematocrit and serum biochemistry indicators like alanine aminotransferase and total bilirubin are common biochemical markers used to measure and assess liver toxicity [106]. Sykes et al. have also demonstrated the use of elemental analysis on skin biopsies to assess the reticuloendothelial

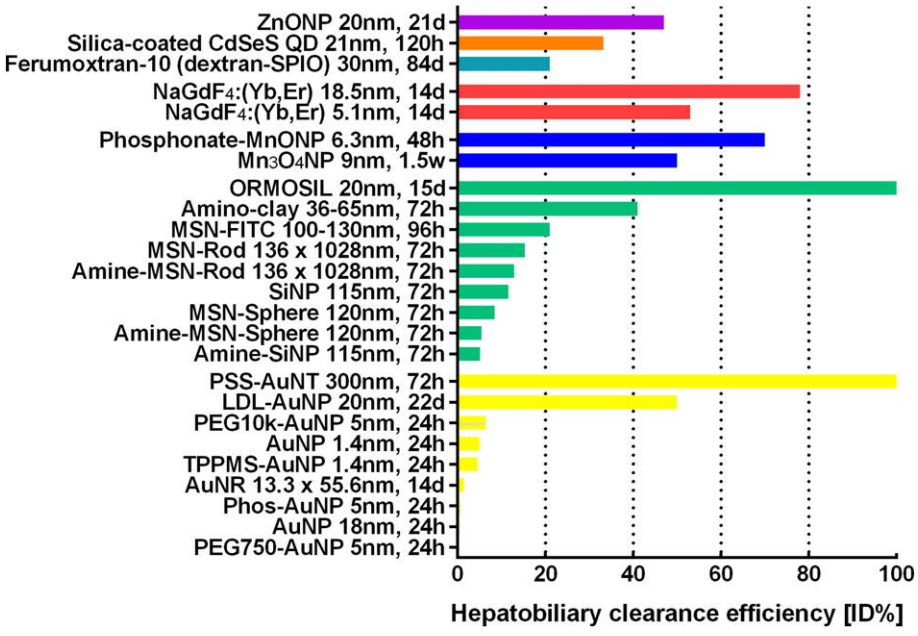

Fig. 4. Hepatobiliary clearance efficiency reported in the literature for a variety of nanoparticle design. Yellow bars represent gold-core based nanoparticle designs, green bars represent silicon-core based nanoparticle designs, blue bar represents manganese-oxide nanoparticle designs, red bar represents upconverting nanoparticle designs, teal bar represents iron oxide nanoparticle designs, orange bar represents QD nanoparticle designs, and purple bar represents zinc oxide nanoparticle designs. Figure was adapted and modified from [4].

Table 3
Nanoparticle hepatobiliary clearance rate and efficiency reported in literature.

Nanoparticle characteristics	Hepatobiliary clearance strategy	Animal system	Detection method	Result	Reference
Silica nanoparticles					
Silica, 50 to 200 nm	None	BALB/c mouse	Fluorescence assay	Elimination of silica in feces within 12 h	[109]
Mesoporous silica, 80 nm	High surface charge by surface silanol groups	Nude mice, or Sprague Dawley rats	ICP–AES + ex vivo fluorescence imaging	Clearance onset ranging from 30 min to more than 3 days based on surface charge	[110]
MSN, 110 nm	None	ICR mice	TEM, confocal microscopy, ICP–AES	Elimination of MSN in feces within 24 h	[111]
ORMOSIL, 20-nm	High surface charge	Athymic nude mice	Fluorescence imaging + PET imaging	100% hepatobiliary clearance after 15 days after IV administration	[98]
Stober SiO_2, 115 nm MSN-Sphere, 120 nm MSN-Nanorod, 136 nm × 1028 nm Stober-Amine MSN-Sphere-Amine MSN-NR-Amine	Varying porosity, geometry, and surface charge	CD-1 mice	Radioactivity assay	5.2–12.9% ID after 72 h	[112]
MSN-FITC, 100-130 nm	None	MCF-7 xenograft tumor-bearing BALB/c nude mice	ICP–AES	21% ID in 96 h	[99]
Amino-clay (3-aminopropyl magnesium phyllosilicate), ~36–65 nm	None	ICR mice	In vivo and ex vivo fluorescence imaging	41% ID in feces in 72 h	[95]
Gadolinium nanoparticles					
Gd-diethylenetriamine-pentaacetate-bis-oleate, 220 nm	None	Rat	MR cholangiography	Entry into biliary tree within 5 min of IV administration	[113]
Gd, 20–25 nm	Cholesterol and HDL	SD rats	MRI, ICP–AES	Enters duodenum after 5 min of administration	[82]
Gold nanoparticles					
Au, 1.4 nm and 18 nm	None	Wistar-Kyoto rats	Radio-tracing	5% ID in feces for 1.4 nm in 24 h; 0.5% ID in feces for 18 nm in 24 h	[101]
Au, 20 nm	LDL	SD rats	Radio-analysis	~50% ID by day 22 after MPS depletion	[85]
PSS-Au nanotubes, 300–700 nm	High surface charge by PSS-ligand	HCT116-tumor bearing CD1 nude mice	Multispectral optoacoustic tomography	Near complete hepatobiliary clearance within 72 h after IV administration	[100]
BSA-Au nanorods, 55.6 nm × 13.3 nm	None	Sprague–Dawley rats	ICP–MS	1.5% ID in 14 days	[103]
TPPMS-Au 1.4 nm	None	Wistar-Kyoto rats	Radioactivity assay	4.6% ID in 24 h	[102]
^{198}Au–Phos, 5 nm ^{198}Au-PEG750, 5 nm ^{198}Au-PEG10k, 5 nm	None	Wistar-Kyoto rats	Radio-analysis	Including GI tract, ^{198}Au–Phos: 0.56% ID in 24 h ^{198}Au-PEG750: 0.27% ID in 24 h ^{198}Au-PEG10k: 6.5% ID in 24 h	[114]
Manganese oxide nanoparticles					
MnO, 6.3 nm	Phosphonate-dendron ligands	BALB/c mice	MRI and INAA	~70% ID eliminated primarily through hepatobiliary clearance within 48 h after IV administration	[94]
Mn_3O_4, 9 nm	None	Kunming white mice	ICP-MS	~50% ID in 1.5 weeks	[115]
Other					
Citrate-coated Ag, ~8 nm	None	SD rats	ICP-MS	Elimination of low levels of Ag in feces within 24 h	[116]
FeO, 7–13 nm	HDL	ApoE KO and WT mice	TEM	HDL is able to cause the hepatobiliary clearance of FeO	[83]
Ferumoxtran-10 (SPIO with dextran), 30 nm	None	SD rats	Radioactivity assay	16–21% ID in 84 days	[97]
Silica-coated CdSeS, 21 nm	None	ICR mice	ICP-MS	33.3% ID in 120 h	[96]
ZnO, 20 nm	None	Wistar-Han rats	INAA	10.5% ID in 24 h, 47% ID in 21 days	[117]
$NaGdF_4$:Yb,Er, 5.1 nm and 18.5 nm	None	LS180 tumor-bearing BALB/c nude mice	ICP–AES	For 5.1 nm: 53% ID in 14 days For 18.5 nm: 78% ID in 14 days	[118]

organ exposure to gold nanoparticles and quantum dots in a minimally invasive yet highly quantitative manner [107]. Mesoporous silica nanoparticles with small aspect ratio (1.5) have been reported to have a net higher hepatobiliary clearance rate compared to those with larger aspect ratio (5), which suggests that hepatobiliary clearance efficiency can be controlled by tuning nanoparticle size and geometry [108]. Nanoparticles are believed to be excreted from hepatocytes in bulk via emptying of lysosomal contents into the biliary canaliculus [85]. Depending on their composition, nanoparticles will be variably excreted into bile, transit through bile ducts, and thus ultimately into the small intestine.

4.2. Nanoparticle sequestration and processing by the MPS is composition-dependent

Clearance through the MPS refers to the removal of nanoparticles from the blood by phagocytic cells in the blood and tissues [119]. Examples of phagocytic cells of the MPS include blood-circulating monocytes,

hepatic Kupffer cells, splenic red pulp and marginal zone macrophages, as well as bone marrow perisinal macrophages and LSECs [86]. Adsorption of serum proteins, in particular opsonization by complement factors, fibrinogen and immunoglobulins, typically triggers nanoparticle processing and clearance from the blood by the MPS [86]. Nanoparticles undergo intracellular degradation inside MPS cells when phagocytosed, and if they are not decomposed by these intracellular processes, they will remain within the cell and be sequestered in the spleen and liver for more than six months [87,104,120,121]. Once the nanoparticle-filled phagocyte dies, there is evidence to suggest that those nanoparticles are taken up again by other phagocytes of the same organ, resulting in a similar total amount of nanoparticles accumulating in growing clusters within a smaller population of Kupffer cells in the liver for example [104]. It has been shown that this bioaccumulation of nanoparticles can result in significant genetic expression changes in the liver (up regulation of toxic metabolic pathways, and down regulation of cell cycle processes-related pathways) even at two months after initial nanoparticle administration [105]. This creates concern about chronic toxicity.

The processing of nanoparticles is dependent on the composition of the nanomaterial. In general, most organic nanoparticles, such as liposomes and polymeric nanoparticles, are readily degraded in the MPS. Liposomes can be degraded by serum proteins during blood circulation or by lipases when endocytosed by various cells. The degradation products of liposomes are their constituent lipid molecules that can be further metabolized by the body. For polymeric nanoparticles, their degradation products include: constituent monomeric units and dissociated polymer chains. If these precursors are smaller than the renal molecular weight cutoff size (~48 kDa) or 5.5 nm (hydrodynamic diameter), they can be eliminated through the renal pathway via the urine [122,123]. For larger constituents, hepatobiliary or MPS clearance is more likely, but their ease of biotransformation in hepatocytes and macrophages represents a toxicity concern. Inorganic nanoparticles generally have relatively more stable cores compared to liposomes and polymeric nanoparticles. There are reports of gold [105], iron oxide [124], and iron oxide-coated gold nanoparticles [125] persisting in the liver even six months after administration as confirmed by elemental analysis and histological observation. However, some types of inorganic nanoparticles may still be degraded in the endolysosomal compartments of phagocytic cells once they are taken up [126]. Zinc oxide nanoparticles have been shown to dissociate in biological media and also be degraded by lysosomes inside cells into their precursor Zn^{2+} ions [127]. The release of Zn^{2+} ions disrupts cellular Zn homeostasis leading to oxidative stress, as well as mitochondrial and lysosomal damage [117,127,128]. Watson et al. demonstrated that zinc oxide nanoparticle dissolution within Kupffer cells leads to the extracellular release of Zn^{2+} ions and subsequent fecal clearance [117]. Their results are also in agreement with the findings from Paek et al. who found that zinc oxide nanoparticles are primarily eliminated from the body via biliary and fecal mechanisms rather than through the renal pathway as expected from established zinc homeostasis [129,130]. Another physiologically important metal known to undergo biliary clearance is manganese [131]. Manganese oxide-based nanoparticles have been shown experimentally to exhibit high hepatobiliary clearance efficiency as well. Chevallier et al. reported approximately 70% of the injected dose was eliminated via feces within 48 h of nanoparticle administration, and Xiao et al. reported roughly 50% of the injected dose within 1.5 weeks [94,115]. The discrepancy may be related to the differential biological processing of divalent and trivalent manganese [131] in the different nanoparticle compositions — MnO [94] versus Mn_3O_4 [115].

By contrast, no defined iron excretory pathway exists in mammals [132,133]. Iron is continuously recycled in the body and any excess is complexed with ferritin protein, found in most cell types of the body but concentrated mostly in the liver and spleen as these are erythrocyte-processing organs for iron extraction [132,133]. Iron oxide-based nanomaterials have been shown to undergo slow degradation in Kupffer cells and become sequestered in the MPS organs in the non-toxic form that is complexed with ferritin and hemosiderin [106,134,135]. The biotransformation of 8 nm Fe_2O_3 nanoparticles into iron-storage protein complexes and their subsequent redistribution from the liver to the spleen over a three month period have been observed [135]. In studies using 12 nm Fe_2O_3 nanoparticles, no breakdown products were visualized by microscopy to be localized within hepatocytes over 84 days [134]. In these studies, the amount of hepatobiliary clearance of iron-oxide nanoparticles was not measured, but their findings do not seem to support the findings by Bourrinet et al., who reported a hepatobiliary clearance efficiency of 16–21% of the injected dose in 84 days.

Intravenously administered silica is usually excreted via the kidneys as silicic acid [136]. Silica nanoparticles are known to degrade into various types of silicic acid depending on porosity, size, and surface chemistry [112,137]. Their degradation has been demonstrated to be mediated by Kupffer cells within 4 weeks of intravenous administration, and they are subsequently released extracellularly for renal clearance [138]. It is noteworthy that renal clearance does not seem to be the only excretory pathway for silica nanoparticles. There have been many reports of a wide variety of silica nanoparticles undergoing hepatobiliary clearance [98,99,109–112]. In particular, Souris et al. and Kumar et al. have attributed the high hepatobiliary clearance efficiency of silica nanoparticles to the high surface charge characteristic of surface silanol groups imparting preferential hepatocyte uptake [98,110]. In addition, it has been shown by TEM and EDX analysis that fully intact silica nanoparticles are present in the feces 24 h after intravenous administration into animals [108,111]. Unexpectedly, researchers have also observed intact silica nanoparticles in the urine as well, which seems highly improbable given the glomerular filtration slit size limit of 5.5 nm [108,111,139]. To this end, the development of a chelator-free ^{89}Zr-labeled mesoporous silica nanoparticle with long term in vivo radiostability for positron emission tomography by Chen et al. may prove useful to elucidate the mechanism behind these contrary renal clearance observations [140].

Lanthanide upconverting nanoparticles are another class of nanomaterials that have been reported to remain intact after hepatobiliary transit. Liu et al. reported the intact fecal excretion of 18.5 nm $NaGdF_4$:Yb,Er nanoparticles both 3 and 14-days post-administration in LS180 tumor-bearing BALB/C nude mice [118]. Due to lack of quantitative evidence for other nanoparticle types, it is unclear if the fecal excretion of intact nanoparticles is a characteristic of certain nanoparticle types only. The more likely case is that nanoparticle integrity following fecal elimination is highly dependent on their degradability. Inorganic nanoparticles with surface chemistries characteristic of high stability or that contain xenobiotic core materials are more likely to resist biotransformation and be eliminated in the feces intact. Conversely, inorganic nanoparticles that are degradable will be eliminated as a combination of aggregates, smaller-sized remnants, ions, and metalloprotein complexes.

4.3. Nanoparticle modifications for enhanced hepatobiliary clearance

For inorganic nanoparticles that are not cleared from the body, one attractive strategy is to target them to hepatocytes and hence access the hepatobiliary clearance route. Several targeting approaches have been widely used and select examples from the literature have been highlighted in Tables 1-3. Galactosyl residues can be conjugated onto delivery systems to take advantage of the high-affinity ASGP hepatocyte surface receptor-mediated uptake [141]. Bergen et al. designed galactose-conjugated gold nanoparticles that have enhanced hepatocyte-specific delivery capabilities in vivo [142]. They also reported a size-dependent effect for hepatocyte-targeting with galactose-conjugated 50 nm gold nanoparticles outperforming 80 nm, 100 nm, and 150 nm gold nanoparticles by a factor of two to three; which suggests that nanoparticle size may also play a critical role in limiting

hepatobiliary clearance [142]. Peptides derived from envelope proteins of hepatitis B have also been demonstrated for hepatocyte-specific delivery of nanoparticles [143].

Another route for accessing hepatobiliary clearance via the hepatocyte is to modify nanoparticle surface charge. Nanomaterials with highly cationic and anionic zeta potentials are cleared efficiently [100,110], as shown in Fig. 5 in a study by Souris et al. They reported shown that the surface charge effect causes differential absorption of lipoproteins onto the nanoparticle corona which then influences elimination pathways and kinetics [98]. Specifically, Cheng et al. demonstrated that apolipoprotein E and IgA bound to a positively charged nanoparticle surface are responsible for their accumulation within hepatocytes using intravital multiphoton fluorescence microscopy [144]. Nanomaterials with positive surface charge are reported to have increased clearance kinetics. Souris et al. reported that the hepatobiliary clearance onset of mesoporous silica nanoparticles with positive zeta potential is less than 30 min post administration, whereas Ye et al. described that highly negatively charged gold nanotubes are cleared after 72 h [100, 110]. It is important to note that the zeta potential of nanoparticles in the body is highly dependent on the physiological environment. The pH of the biliary tract and duodenum is relatively alkaline (~7–7.7 for humans, ~8.5 for rodents), whereas the distal small intestine is more acidic (~4–6) and gradually increases back to physiologically neutral (~7.4) at the rectum [145,146]. The pH of the gastrointestinal tract is also highly dependent on the fasting state. Nanomaterial designs that rely on surface charge for hepatobiliary clearance should have a surface chemistry design that takes into account this spatial and temporal variance in pH. The dichotomy from the polarity of surface charge may be related to the preferential uptake of positively charged nanoparticles by hepatocytes and negatively charged nanoparticles by Kupffer cells [144]. Other strategies for hepatobiliary clearance include the conjugation of nanoparticles with phosphonate dendrons (repetitively branched molecules containing phosphonate moieties) [94]. A variety of nanomaterials, such as magnesium oxide nanoparticles and iron oxide nanoparticles, have been shown to be efficiently cleared via the hepatobiliary system when conjugated to dendrons due to their increased colloidal stability and avoidance of MPS sequestration [94, 147,148]. Lipka et al. investigated the effect of PEGylation on the excretion of 5 nm gold nanoparticles in Wistar-Kyoto rats and reported that gold nanoparticles surface-modified with PEG10k exhibited a higher rate of hepatobiliary clearance within 24 h post nanoparticle administration [114]. Interestingly, gold nanoparticles surface-modified with PEG750 were cleared in the feces less efficiently than bare gold nanoparticles, which suggests the configuration of surface passivation molecules is also important. A call for studies with increased sampling and over a longer duration is needed to compare the effect of nanoparticle surface passivation on hepatobiliary clearance before any general conclusions can be drawn. In addition, Lipka et al. reported the

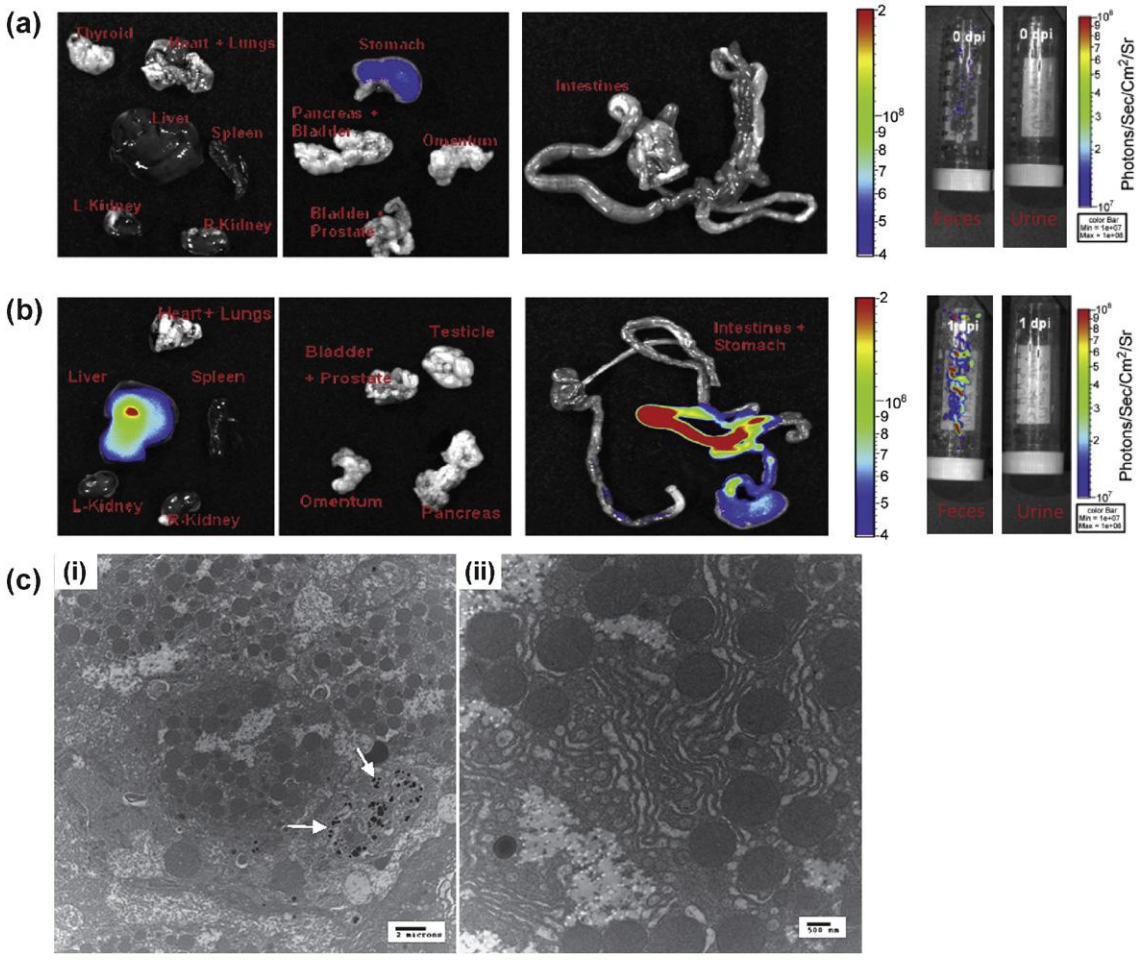

Fig. 5. Ex vivo fluorescence images of excised organs, feces, and urine from (a) control mouse and (b) treated mouse approximately 3 h post tail vein injection of indocyanine green-conjugated mesoporous silica nanoparticles (MSN-amino-ICG). There is significantly more MSN-amino-ICG in the liver, intestine, and feces of the nanoparticle-treated mouse, suggesting a primarily hepatobiliary clearance pathway for the engineered nanoparticle. Transmission electron microscopy images of liver sections from the treated mouse (c left) 10 min and (c right) 3 days following tail vein injection of MSN-amino-ICG. Many MSNs can be seen in liver cells at 10 min, while there are none found 3 days later, suggesting fairly quick hepatobiliary clearance from the liver. Reprinted with permission from [110]. Copyright 2010 Elsevier.

hydrodynamic diameters of Au-PEG750 and Au-PEG10K nanoparticles were 21 and 31 nm, respectively (the 5 nm gold core size was identical for both nanoparticles). It is unclear in the literature whether hydrodynamic size or the molecular weight of the PEG chain is the predominating factor in determining the distribution of nanoparticle uptake between Kupffer cells and hepatocytes [114].

Despite these strategies, Kupffer cells rapidly sequester most of the nanoparticles and remain a significant barrier in engineered nanomaterial–hepatocyte interaction [149]. Some strategies to limit or prevent Kupffer cell sequestration are summarized in the subsequent section and may impact the efficacy of the nanoparticle clearance through the hepatobiliary route. It is worth mentioning that alone, the delivery of nanomaterials to the hepatocyte does not guarantee subsequent transcytosis and elimination by the biliary process, and this process is not well-characterized and the mechanism is not understood.

5. Preventing nanoparticle liver interactions: moving toward nanotherapeutics

With the majority of administered nanoparticles residing in hepatic tissues, this creates a significant challenge toward the development of nanotherapeutics and imaging agents due to low accumulation in the desired diseased tissue. Within the last few years, strategies have been proposed to delay, reduce or entirely circumvent the phagocytoses of nanoparticles by macrophages in addition to grafting anti-fouling coatings such as PEG to the nanoparticle surface. Fig. 6 illustrates the current methods that are being used or proposed to reduce nanoparticle sequestration by the liver and resident cells.

5.1. Shape modification of nanoparticles

Shape modification of nanoparticles can influence the behavior of nanoparticles in the bloodstream and their distribution. However, there is no firm data to suggest that one shape is definitively better for reducing sequestration by the MPS. Many research groups have reported that rod-shaped nanoparticles can significantly reduce the uptake by the MPS when compared to spherical shapes [150–153]. Interestingly, worm-like particles with very high aspect ratios seem to exhibit negligible uptake by macrophages and have increased blood circulation [88,150,154]. This shape-based inhibition of phagocytosis is due to the limitation of accessible binding sites between particles and macrophages. Based on these principles, filomicelles with high aspect ratios (>10) and longitudinal length of 10 μm were successfully retained in the blood for up to one week [88,150]. In addition, worm-like polystyrene particles with high aspect ratios (>20) show negligible phagocytosis by macrophages [154]. Modeling of receptor mediated nanoparticle uptake has suggested that internalization requires at least 2–20 receptor–ligand interactions with the phagocytic cell [23]. The smaller radius of curvature of rod-shaped nanoparticles can reduce interactions with macrophages and subsequent phagocytosis [154]. Clearance of these high aspect ratio polystyrene nanoparticles remains challenging [155]. They are not degradable or easily broken into smaller subunits for renal or hepatobiliary clearance. At the same time, their microscale size makes it difficult for macrophages to phagocytose.

5.2. Modulus of nanoparticles

Mechanical properties (especially elasticity and deformability) of nanoparticles can also influence the efficiency of phagocytosis and blood circulation times [11]. Beningo and Wang [156] reported that macrophages prefer to take up rigid particles rather than softer counterparts. Hydrogel particles with tunable elasticity were synthesized with a similar size and shape to red blood cells [157]. The results show that by decreasing the nanoparticle modulus by eight-fold, the nanoparticle blood half-life can be increased by a factor of thirty. Therefore, soft particles may be advantageous since they can minimize the sequestration by the MPS.

5.3. Surface modification of nanoparticles

To inhibit the internalization of nanoparticles by the MPS when intravenously administered, conjugation of neutral PEG ligands

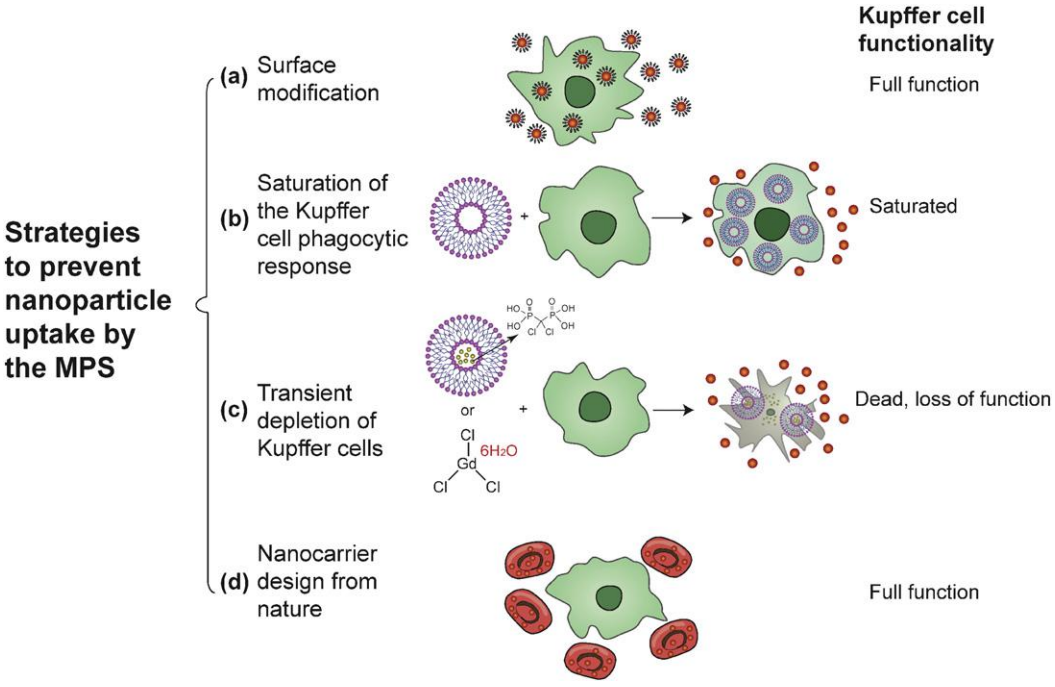

Fig. 6. Schematic of strategies to prevent nanoparticle uptake by the MPS, in particular by Kupffer cells. The strategies can be summarized as (a) surface modification, (b) saturation of the Kupffer cell phagocytic response, (c) transient depletion of Kupffer cells, and (d) nanocarrier design from nature. The functionalities of Kupffer cells following different strategies are also summarized.

on the nanoparticle surface has been widely used in nanotechnology [2,9,13,158] (Fig. 6a). However, the bioactivity of targeting ligands on PEGylated nanoparticles can be significantly reduced. This can be overcome by designing the nanoparticle surface with different sized PEG molecules [159]. Bartneck et al. [160] studied nanoparticle uptake using human primary leukocytes and reported that uptake can be delayed or inhibited for all particle geometries by surface modification using PEG. Another strategy other than PEGylation, nanoparticle conjugation with zwitterionic polymers (such as poly(carboxybetaine)) may offer improved colloidal stability by resisting the nonspecific adsorption of serum proteins [161–163].

5.4. Saturation of the Kupffer cell phagocytic response

The principle of saturating the receptors of Kupffer cells with decoy and nontoxic nanoparticles prior to administration of nanotherapeutics can enhance their delivery to diseased tissues. Liposomes comprised of phosphatidylcholine and cholesterol were used to saturate the phagocytosis of macrophages [164] (Fig. 6b). This blockade was noted to initialize within 90 min after intravenous administration and resulted in an increased delivery window that lasted up to 48 h. Using a single administration of these liposomes, the accumulation of PEGylated nanoparticles in a human prostate cancer xenograft model increased by two-fold compared to controls. This blockade approach is safe and does not damage the innate immunity as no weight loss, impairment of liver function or RES-mediated host defense in the mice was noted [164]. The limit of this strategy is that the phagocytic functionality of Kupffer cells were not fully saturated as reflected by only a two-fold improved tumor accumulation. Once liposomes are engulfed by Kupffer cells, they accumulate in a phagosome, fuse with a lysosome and then are subsequently digested by lysosomal enzymes [165]. Future developments may consider the use of nanoparticles comprised of materials that have slower degradation rates.

5.5. Transient depletion of macrophages

A more aggressive method to manipulate the microenvironment of the sinusoid is through an approach developed by Van Rooijen et al. [166,167]. This is commonly referred to as the macrophage 'suicide' technique. This technique is premised around the use of liposomes to encapsulate dichloromethylene-bisphosphonate or clodronate (Fig. 6c). When these liposomes are taken up by macrophages, the phospholipid bilayers of the liposomes are digested by lysosomal phospholipases to release clodronate to inhibit ADP/ATP translocase in the mitochondria and ultimately trigger the apoptosis of these macrophages [168]. The advantage of this approach is that clodronate liposomes are not taken up by non-phagocytic cells. After macrophage apoptosis, the remaining clodronate drug is removed from circulation by the renal system, leading to an extremely short half-life in the bloodstream. Hepatic tissues have dramatically reduced numbers of Kupffer cells after intravenous administration of liposomal clodronate. It is noteworthy that at higher dosages, depletion of splenic macrophages may also result in splenomegaly [169].

Nanoparticle biodistribution following Kupffer cell depletion by clodronate liposomes has been studied in mice [170]. PEGylated liposomal doxorubicin or Doxil nanoparticles showed improved accumulation in a xenograft human pancreatic tumor model and inhibited tumor growth [171]. Additionally, this suicide strategy yielded a higher accumulation of SPIONs in MDA-MB-435 xenograft tumors in mice [172]. Similar improvements in biodistribution and reduced liver accumulation of QDs were also reported using transient macrophage depletion [173]. Taken together, these results indicate that temporary suppression or depletion of macrophages in the liver using clodronate liposomes can enhance the nanoparticle circulation in the blood, and improve their accumulation in desired diseased tissues.

Similar to liposomal clodronate, gadolinium chloride ($GdCl_3$) has also been used to inhibit and/or deplete the function of Kupffer cells [174], as shown in Fig. 6c. Using $GdCl_3$, the reduced phagocytic activity of Kupffer cells has been reported [175,176]. The phagocytosis suppression is due to the inhibition of calcium transport across the cell membrane by the Gd (III) ion [175]. Histological sections of hepatic tissue demonstrated that a significant amount of Kupffer cells were removed, indicating these Kupffer cells were not only suppressed but some of them were eliminated [176]. Furthermore, some of the red pulp macrophages in the spleen were also eliminated, but the repopulation of splenic macrophages is much faster [176]. In a study by Diagaradjane et al. [177], QDs were shown to have increased blood circulation time and amplified florescence signals at tumor tissues after pre-treatment with $GdCl_3$ as shown in Fig. 7 [177].

While these chemical agents may prevent the interaction between Kupffer cells and nanoparticles, they have no effect on LSECs uptake and thus may have greater utility in preventing the liver sequestration of larger nanomaterials. It has been noted that $GdCl_3$ can also cause hepatic alterations by eliminating Kupffer cells and increasing cytokine release, including tumor necrosis factor α and interleukin-1 [174]. Moreover, Kupffer cells and other tissue resident macrophages play an important role in innate immunity. Depletion of these macrophages may reduce the integrity of the immune system and could possibly lead to increased susceptibility to infection by pathogens. While attractive, these transient depletion strategies are not well-characterized for their safety and studies investigating dose–efficacy relationships and their concurrent effects on innate immunity are not available.

5.6. Intrinsic evasiveness: using and modeling nanocarrier design from nature

Bio-inspired approaches have been studied for reducing nanoparticle uptake by the liver [178–184] (Fig. 6d). These techniques use circulating red blood cells, leukocytes, and monocytes (precursors to tissue adherent macrophages). Nanoparticles non-covalently attached on erythrocytes avoided rapid clearance by the liver and other macrophages in the body [179]. With this cellular "hitchhiking" method, nanoparticles exhibited a three-fold higher circulation half-life and seven-fold higher accumulation in lung tissues. Nanoporous silicon particles coated with leukocyte membranes can evade the immune system by reducing the degree of opsonization by serum proteins [180]. These nanoparticles exhibited enhanced blood circulation and accumulation at the location of diseased tissues. Furthermore, monocytes/macrophages served as 'Trojan horses' to deliver nanoparticles to solid tumors while minimizing their sequestration by the MPS [181,182]. For example, gold nanoshells were loaded into tumor associated macrophages through phagocytosis in cell culture, injected into the animal, and released by laser excitation [181]. All of these are creative strategies to circumvent the interaction of nanoparticles with the liver and more studies are required to validate the real-world utility of such techniques.

6. Conclusion

The liver presents one of the biggest problems for using nanoparticles clinically. The sequestration of nanoparticles by the liver prevents them from targeting extrahepatic diseased tissue. While there are many studies on the topic of particle-to-liver interactions in the 1970s and 1980s, the conclusions established in that timeframe may not be fully applicable to current nanoparticle technologies. As the size of a particle decreases to less than 100 nm, they are on the same scale as many biological molecules. They may have access to different tissue and cellular structures within the liver and may have different accumulation patterns. Yet, there have been relatively few studies on the new generation of nanoparticles with the liver in the last 10–20 years. This new generation of nanoparticles can be synthesized with higher precision in the sub-100 nm size range and the surface chemistry can be

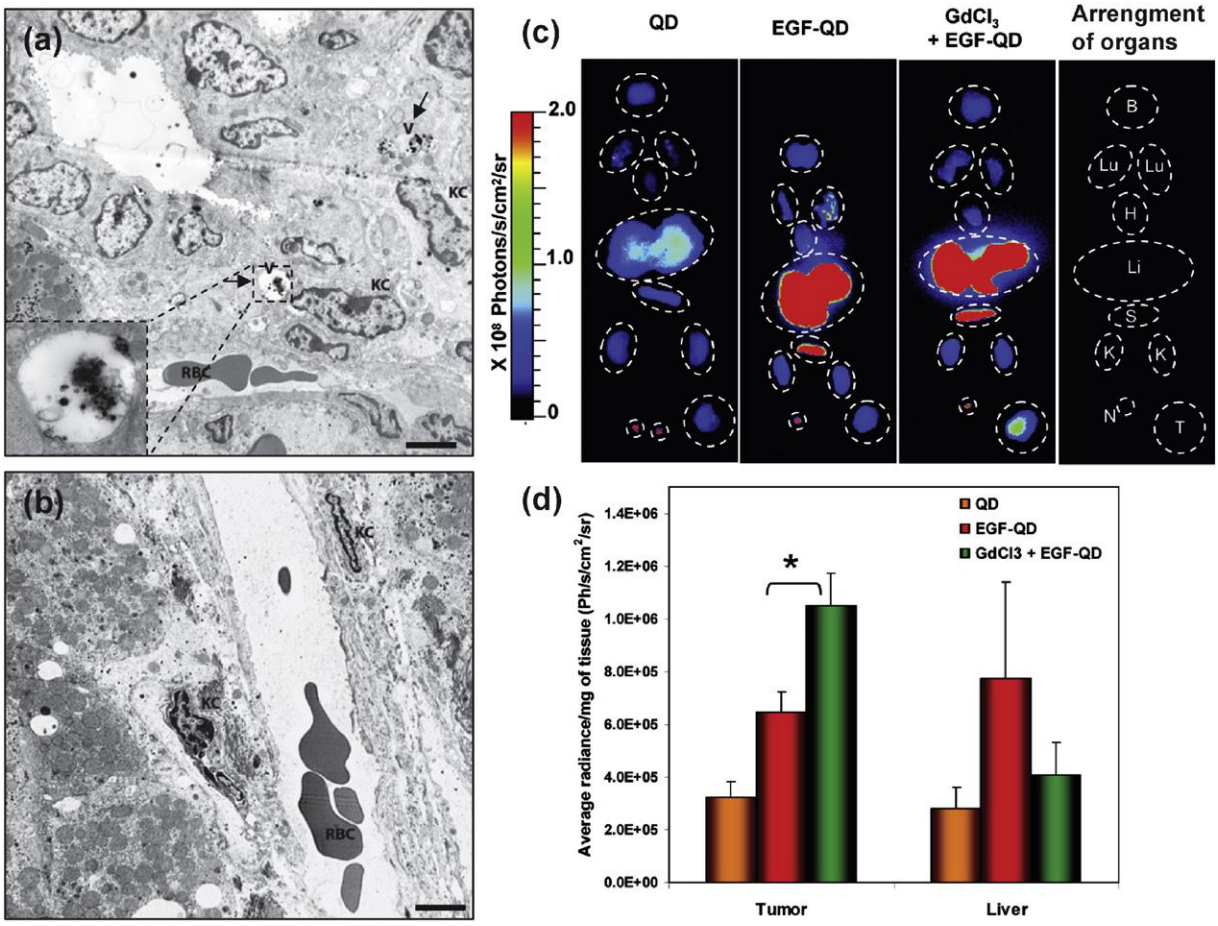

Fig. 7. Transmission electron microscopy image of mice liver tissue 4 h after (a) epidermal growth factor (EGF) QD administration. The arrows in (a) represent the accumulation of QDs in Kupffer cells, and the magnified inset represents the vesicles containing the QDs. (b) $GdCl_3$ pretreatment followed by EGF-QDs administration. No nanoparticles were found in Kupffer cells when $GdCl_3$ was used to suppress phagocytic activity. The labels V, KC, and RBC represent the vesicles, Kupffer cells, and red blood cells, respectively (scale bar = 5 μm). Ex vivo fluorescence images of organs 4 h after (c) QD administration, EGF-QD administration, and $GdCl_3$ pretreatment followed by EGF-QD administration. Schematic illustrates ex vivo fluorescence images of organs, B, Lu, H, Li, S, K, N, and T represent the brain, lungs, heart, liver, spleen, kidney, lymph node, and tumor, respectively. $GdCl_3$ prevented nanoparticle accumulation in Kupffer cells that translated to improved tumour accumulation. The corresponding fluorescence signals from the tumor and liver are represented in (d). A significantly higher fluorescence signal was found in the tumor while lower fluorescence is in the liver with $GdCl_3$ pretreatment followed by EGF-QD administration compared to the only EGF-QD injection, which shows the effect of phagocytosis blocking. Adapted with permission from [177]. Copyright 2010 American Chemical Society.

decorated with different types of molecules for different functions in vivo. Thus, there is a need for a better understanding of the interactions of nanoparticles with sizes less than 100 nm with the liver from the organ to cell perspective. Furthermore, there should be a focus on identifying nanoparticle–liver interaction "metrics" that would guide the development of nanomedicine. For example, it would be useful to quantitatively determine a mathematical relationship between reduction in Kupffer cells or clearance timeframes with nanoparticle accumulation in diseased tissues. Finally, the research community should develop and confirm whether many of the proposed new and innovative solutions can solve the nanoparticle–liver sequestration problem. Moving forward, the community needs to focus on the major biological barrier that is currently plaguing the field of nanomedicine.

Acknowledgments

WCWC would like to acknowledge the Canadian Institute of Health Research (CIHR) (MOP-130143, RMF-111623), Natural Sciences and Engineering Research Council (NSERC) (2015-06397), and Prostate Cancer Canada (D2014-12) for supporting his research program. WCWC and IDM would both like to thank CIHR for a shared grant (GCS 105653-1). YNZ would like to thank Ministry of Training Colleges and Universities for provision of an Ontario Graduate Scholarship, the Wildcat Foundation graduate scholarship, the Paul and Sally Wang distinguished graduate scholarship from University of Toronto and an Alexander Graham Bell Canada graduate scholarship by NSERC for their support. WP would also like to acknowledge the Cecil Yip Doctoral Research Award, Barbara & Frank Milligan Graduate Fellowship, and the CIHR Frederick Banting and Charles Best Canada graduate scholarship for provision of scholarships.

References

[1] L.Y. Chou, K. Ming, W.C. Chan, Strategies for the intracellular delivery of nanoparticles, Chem. Soc. Rev. 40 (2011) 233–245.
[2] T. Sun, Y.S. Zhang, B. Pang, D.C. Hyun, M. Yang, Y. Xia, Engineered nanoparticles for drug delivery in cancer therapy, Angew. Chem. Int. Ed. 53 (2014) 12320–12364.
[3] W. Poon, X. Zhang, J. Nadeau, Nanoparticle drug formulations for cancer diagnosis and treatment, Crit. Rev. Oncog. 19 (2014) 223–245.
[4] M. Yu, J. Zheng, Clearance pathways and tumor targeting of imaging nanoparticles, ACS Nano 9 (2015) 6655–6674.
[5] S.R.Z. Abdel-Misih, M. Bloomston, Liver anatomy, Surg. Clin. North Am. 90 (2010) 643–653.
[6] L.T. Hoekstra, W. de Graaf, G.A.A. Nibourg, M. Heger, R.J. Bennink, B. Stieger, T.M. van Gulik, Physiological and biochemical basis of clinical liver function tests, Ann. Surg. 257 (2013) 27–36.
[7] G. Ghibellini, E.M. Leslie, K.L.R. Brouwer, Methods to evaluate biliary excretion of drugs in humans: an updated review, Mol. Pharm. 3 (2006) 198–211.
[8] S.M. Pond, T.N. Tozer, First-pass elimination basic concepts and clinical consequences, Clin. Pharmacokinet. 9 (1984) 1–25.
[9] H. Wang, C.A. Thorling, X. Liang, K.R. Bridle, J.E. Grice, Y. Zhu, D.H.G. Crawford, Z.P. Xu, X. Liu, M.S. Roberts, Diagnostic imaging and therapeutic application of nanoparticles targeting the liver, J. Mater. Chem. B 3 (2015) 939–958.

[10] V. Racanelli, B. Rehermann, The liver as an immunological organ, Hepatology 43 (2006) S54–S62.
[11] N. Bertrand, J.-C. Leroux, The journey of a drug-carrier in the body: an anatomo-physiological perspective, J. Control. Release 161 (2012) 152–163.
[12] S.L. Friedman, Hepatic stellate cells: protean, multifunctional, and enigmatic cells of the liver, Physiol. Rev. 88 (2008) 125–172.
[13] L. Li, H. Wang, Z.Y. Ong, K. Xu, P.L.R. Ee, S. Zheng, J.L. Hedrick, Y.-Y. Yang, Polymer- and lipid-based nanoparticle therapeutics for the treatment of liver diseases, Nano Today 5 (2010) 296–312.
[14] L.H. Reddy, P. Couvreur, Nanotechnology for therapy and imaging of liver diseases, J. Hepatol. 55 (2011) 1461–1466.
[15] N. Mishra, N.P. Yadav, V.K. Rai, P. Sinha, K.S. Yadav, S. Jain, S. Arora, Efficient hepatic delivery of drugs: novel strategies and their significance, Biomed. Res. Int. 2013 (2013) 382184.
[16] C.A. Janeway, P. Travers, M. Walport, M.J. Shlomchik, The Front Line of Host Defense, Garland Science, 2001.
[17] B.W. Doble, J.R. Woodgett, GSK-3: tricks of the trade for a multi-tasking kinase, J. Cell Sci. 116 (2003) 1175–1186.
[18] L.C. Davies, S.J. Jenkins, J.E. Allen, P.R. Taylor, Tissue-resident macrophages, Nat. Immunol. 14 (2013) 986–995.
[19] A. Aderem, D.M. Underhill, Mechanisms of phagocytosis in macrophages, Annu. Rev. Immunol. 17 (1999) 593–623.
[20] C.D. Walkey, J.B. Olsen, H. Guo, A. Emili, W.C.W. Chan, Nanoparticle size and surface chemistry determine serum protein adsorption and macrophage uptake, J. Am. Chem. Soc. 134 (2012) 2139–2147.
[21] H.C. Fischer, T.S. Hauck, A. Gómez-Aristizábal, W.C.W. Chan, Exploring primary liver macrophages for studying quantum dot interactions with biological systems, Adv. Mater. 22 (2010) 2520–2524.
[22] M.A. Dobrovolskaia, S.E. McNeil, Immunological properties of engineered nanomaterials, Nat. Nanotechnol. 2 (2007) 469–478.
[23] O. Lunov, V. Zablotskii, T. Syrovets, C. Röcker, K. Tron, G.U. Nienhaus, T. Simmet, Modeling receptor-mediated endocytosis of polymer-functionalized iron oxide nanoparticles by human macrophages, Biomaterials 32 (2011) 547–555.
[24] R.G. Thurman, Mechanisms of hepatic toxicity II. Alcoholic liver injury involves activation of Kupffer cells by endotoxin, Am. J. Phys. 275 (1998) G605–G611.
[25] M.E. Gershwin, J.M. Vierling, M.P. Manns, Liver Immunology. Principles and Practice, Springer International Publishing, 2014.
[26] B. Smedsrød, Clearance function of scavenger endothelial cells, Comp. Hepatol. 3 (2004) S22.
[27] J.A.A.M. Kamps, H. Morselt, P.J. Swart, D. Keijer, G.L. Scherphof, Massive targeting of liposomes, surface-modified with anionized albumins, to hepatic endothelial cells, Proc. Natl. Acad. Sci. U. S. A. 94 (1997) 11681–11685.
[28] S.R. Popielarski, S. Hu-Lieskovan, S.W. French, T.J. Triche, M.E. Davis, A nanoparticle-based model delivery system to guide the rational design of gene delivery to the liver. 2. In vitro and in vivo uptake results, Bioconjug. Chem. 16 (2005) 1071–1080.
[29] C. Yin, K.J. Evason, K. Asahina, D.Y.R. Stainier, Hepatic stellate cells in liver development, regeneration, and cancer, J. Clin. Invest. 123 (2013) 1902–1910.
[30] L. Beljaars, G. Molema, D. Schuppan, A. Geerts, P.J. Bleser, B. Weert, D.K.F. Meijer, K. Poelstra, Successful targeting to rat hepatic stellate cells using albumin modified with cyclic peptides that recognize the collagen type VI receptor, J. Biol. Chem. 275 (2000) 12743–12751.
[31] S.-L. Du, H. Pan, W.-Y. Lu, J. Wang, J. Wu, J.-Y. Wang, Cyclic Arg–Gly–Asp peptide-labeled liposomes for targeting drug therapy of hepatic fibrosis in rats, J. Pharmacol. Exp. Ther. 322 (2007) 560–568.
[32] H.T.T. Duong, Z. Dong, L. Su, C. Boyer, J. George, T.P. Davis, J. Wang, The use of nanoparticles to deliver nitric oxide to hepatic stellate cells for treating liver fibrosis and portal hypertension, Small 11 (2015) 2291–2304.
[33] R.J. Fallon, A.L. Schwartz, Receptor-mediated delivery of drugs to hepatocytes, Adv. Drug Deliv. Rev. 4 (1989) 49–63.
[34] E.L. Romero, M.-J. Morilla, J. Regts, G.A. Koning, G.L. Scherphof, On the mechanism of hepatic transendothelial passage of large liposomes, FEBS Lett. 448 (1999) 193–196.
[35] W.-W. Qi, H.-Y. Yu, H. Guo, J. Lou, Z.-M. Wang, P. Liu, A. Sapin-Minet, P. Maincent, X.-C. Hong, X.-M. Hu, Y.-L. Xiao, Doxorubicin-loaded glycyrrhetinic acid modified recombinant human serum albumin nanoparticles for targeting liver tumor chemotherapy, Mol. Pharm. 12 (2015) 675–683.
[36] Q. Tian, C.-N. Zhang, X.-H. Wang, W. Wang, W. Huang, R.-T. Cha, C.-H. Wang, Z. Yuan, M. Liu, H.-Y. Wan, H. Tang, Glycyrrhetinic acid-modified chitosan/poly(ethylene glycol) nanoparticles for liver-targeted delivery, Biomaterials 31 (2010) 4748–4756.
[37] M. Negishi, A. Irie, N. Nagata, A. Ichikawa, Specific binding of glycyrrhetinic acid to the rat liver membrane, Biochim. Biophys. Acta Biomembr. 1066 (1991) 77–82.
[38] A. Lin, Y. Liu, Y. Huang, J. Sun, Z. Wu, X. Zhang, Q. Ping, Glycyrrhizin surface-modified chitosan nanoparticles for hepatocyte-targeted delivery, Int. J. Pharm. 359 (2008) 247–253.
[39] F. Wu, S.A. Wuensc, M. Azadniv, M.R. Ebrahimkhani, I.N. Crispe, Galactosylated LDL nanoparticles: a novel targeting delivery system to deliver antigen to macrophages and enhance antigen specific T cell responses, Mol. Pharm. 6 (2009) 1506–1517.
[40] P. Opanasopit, M. Sakai, M. Nishikawa, S. Kawakami, F. Yamashita, M. Hashida, Inhibition of liver metastasis by targeting of immunomodulators using mannosylated liposome carriers, J. Control. Release 80 (2002) 283–294.
[41] Y. Higuchi, S. Kawakami, M. Oka, Y. Yabe, F. Yamashita, M. Hashida, Intravenous administration of mannosylated cationic liposome/NFkB decoy complexes effectively prevent LPS-induced cytokine production in a murine liver failure model, FEBS Lett. 580 (2006) 3706–3714.
[42] A. Akhter, Y. Hayashi, Y. Sakurai, N. Ohga, K. Hida, H. Harashima, Ligand density at the surface of a nanoparticle and different uptake mechanism: two important factors for successful siRNA delivery to liver endothelial cells, Int. J. Pharm. 475 (2014) 227–237.
[43] B.T. Kren, G.M. Unger, L. Sjeklocha, A.A. Trossen, V. Korman, B.M. Diethelm-Okita, M.T. Reding, C.J. Steer, Nanocapsule-delivered sleeping beauty mediates therapeutic factor VIII expression in liver sinusoidal endothelial cells of hemophilia A mice, J. Clin. Invest. 119 (2009) 2086–2099.
[44] M.-Y. Lee, J.-A. Yang, H.S. Jung, S. Beack, J.E. Choi, W. Hur, H. Koo, K. Kim, S.K. Yoon, S.K. Hahn, Hyaluronic acid–gold nanoparticle/interferon α complex for targeted treatment of hepatitis C virus infection, ACS Nano 6 (2012) 9522–9531.
[45] J.E. Adrian, J.A.A.M. Kamps, K. Poelstra, G.L. Scherphof, D.K.F. Meijer, Y. Kaneda, Delivery of viral vectors to hepatic stellate cells in fibrotic livers using HVJ envelopes fused with targeted liposomes, J. Drug Target. 15 (2007) 75–82.
[46] F.-Q. Li, H. Su, X. Chen, X.-J. Qin, J.-Y. Liu, Q.-G. Zhu, J.-H. Hu, Mannose 6-phosphate-modified bovine serum albumin nanoparticles for controlled and targeted delivery of sodium ferulate for treatment of hepatic fibrosis, J. Pharm. Pharmacol. 61 (2009) 1155–1161.
[47] G. Patel, G. Kher, A. Misra, Preparation and evaluation of hepatic stellate cell selective, surface conjugated, peroxisome proliferator-activated receptor-gamma ligand loaded liposomes, J. Drug Target. 20 (2012) 155–165.
[48] J.E. Adrian, K. Poelstra, G.L. Scherphof, D.K.F. Meijer, A.-M. van Loenen-Weemaes, C. Reker-Smit, H.W.M. Morselt, P. Zwiers, J.A.A.M. Kamps, Effects of a new bioactive lipid-based drug carrier on cultured hepatic stellate cells and liver fibrosis in bile duct-ligated rats, J. Pharmacol. Exp. Ther. 321 (2007) 536–543.
[49] F. Li, Q.-h. Li, L.-y. Wang, C.-y. Zhan, C. Xie, W.-y. Liu, Effects of interferon-gamma liposomes targeted to platelet-derived growth factor receptor–beta on hepatic fibrosis in rats, J. Control. Release 159 (2012) 261–270.
[50] O. Mezghrani, Y. Tang, X. Ke, Y. Chen, D. Hu, J. Tu, L. Zhao, N. Bourkaib, Hepatocellular carcinoma dually-targeted nanoparticles for reduction triggered intracellular delivery of doxorubicin, Int. J. Pharm. 478 (2015) 553–568.
[51] Y. Sato, K. Murase, J. Kato, M. Kobune, T. Sato, Y. Kawano, R. Takimoto, K. Takada, K. Miyanishi, T. Matsunaga, T. Takayama, Y. Niitsu, Resolution of liver cirrhosis using vitamin A-coupled liposomes to deliver siRNA against a collagen-specific chaperone, Nat. Biotechnol. 26 (2008) 431–442.
[52] Z. Zhang, C. Wang, Y. Zha, W. Hu, Z. Gao, Y. Zang, J. Chen, J. Zhang, L. Dong, Corona-directed nucleic acid delivery into hepatic stellate cells for liver fibrosis therapy, ACS Nano 9 (2015) 2405–2419.
[53] Q.-B. Wang, Y. Han, T.-T. Jiang, W.-M. Chai, K.-M. Chen, B.-Y. Liu, L.-F. Wang, C. Zhang, D.-B. Wang, MR imaging of activated hepatic stellate cells in liver injured by CCl4 of rats with integrin-targeted ultrasmall superparamagnetic iron oxide, Eur. J. Radiol. 21 (2011) 1016–1025.
[54] K.M. Selim, Y.-S. Ha, S.-J. Kim, Y. Chang, T.-J. Kim, G. Ho Lee, I.-K. Kang, Surface modification of magnetite nanoparticles using lactobionic acid and their interaction with hepatocytes, Biomaterials 28 (2007) 710–716.
[55] C.-M. Lee, H.-J. Jeong, E.-M. Kim, D.W. Kim, S.T. Lim, H.T. Kim, I.-K. Park, Y.Y. Jeong, J.W. Kim, M.-H. Sohn, Superparamagnetic iron oxide nanoparticles as a dual imaging probe for targeting hepatocytes in vivo, Magn. Reson. Med. 62 (2009) 1440–1446.
[56] J. Peng, K. Wang, W. Tan, X. He, C. He, P. Wu, F. Liu, Identification of live liver cancer cells in a mixed cell system using galactose-conjugated fluorescent nanoparticles, Talanta 71 (2007) 833–840.
[57] Z. Xu, L. Chen, W. Gu, Y. Gao, L. Lin, Z. Zhang, Y. Xi, Y. Li, The performance of docetaxel-loaded solid lipid nanoparticles targeted to hepatocellular carcinoma, Biomaterials 30 (2009) 226–232.
[58] Y. Yang, S.-X. Yuan, L.-H. Zhao, C. Wang, J.-S. Ni, Z.-G. Wang, C. Lin, M.-C. Wu, W.-P. Zhou, Ligand-directed stearic acid grafted chitosan micelles to increase therapeutic efficacy in hepatic cancer, Mol. Pharm. 12 (2015) 644–652.
[59] K.W. Yang, X.R. Li, Z.L. Yang, P.Z. Li, F. Wang, Y. Liu, Novel polyion complex micelles for liver-targeted delivery of diammonium glycyrrhizinate: in vitro and in vivo characterization, J. Biomed. Mater. Res. A 88 (2008) 140–148.
[60] J. Wu, T.-M. Sun, X.-Z. Yang, J. Zhu, X.-J. Du, Y.-D. Yao, M.-H. Xiong, H.-X. Wang, Y.-C. Wang, J. Wang, Enhanced drug delivery to hepatocellular carcinoma with a galactosylated core–shell polyphosphoester nanogel, Biomater. Sci. 1 (2013) 1143.
[61] F. Yu, T. Jiang, J. Zhang, L. Cheng, S. Wang, Galactosylated liposomes as oligodeoxynucleotides carrier for hepatocyte-selective targeting, Pharmazie 62 (2007).
[62] N. Jiang, X. Zhang, X. Zheng, D. Chen, Y. Zhang, L.K.S. Siu, H.-B. Xin, R. Li, H. Zhao, N. Riordan, T.E. Ichim, D. Quan, A.M. Jevnikar, G. Chen, W. Min, Targeted gene silencing of TLR4 using liposomal nanoparticles for preventing liver ischemia reperfusion injury, Am. J. Transplant. 11 (2011) 1835–1844.
[63] N. Jiang, X. Zhang, X. Zheng, D. Chen, K. Siu, H. Wang, T.E. Ichim, D. Quan, V. McAlister, G. Chen, W.-P. Min, A novel in vivo siRNA delivery system specifically targeting liver cells for protection of ConA-induced fulminant hepatitis, PLoS One 7 (2012) e44138.
[64] S. Gupta, A. Agarwal, N.K. Gupta, G. Saraogi, H. Agrawal, G.P. Agrawal, Galactose decorated PLGA nanoparticles for hepatic delivery of acyclovir, Drug Dev. Ind. Pharm. 39 (2013) 1866–1873.
[65] M. Cheng, B. He, T. Wan, W. Zhu, J. Han, B. Zha, H. Chen, F. Yang, Q. Li, W. Wang, H. Xu, T. Ye, 5-Fluorouracil nanoparticles inhibit hepatocellular carcinoma via activation of the p53 pathway in the orthotopic transplant mouse model, PLoS One 7 (2012) e47115.

[66] D. Zheng, C. Duan, D. Zhang, L. Jia, G. Liu, Y. Liu, F. Wang, C. Li, H. Guo, Q. Zhang, Galactosylated chitosan nanoparticles for hepatocyte-targeted delivery of oridonin, Int. J. Pharm. 436 (2012) 379–386.
[67] H.-F. Liang, S.-C. Chen, M.-C. Chen, P.-W. Lee, C.-T. Chen, H.-W. Sung, Paclitaxel-loaded poly(gamma-glutamic acid)-poly(lactide) nanoparticles as a targeted drug delivery system against cultured HepG2 cells, Bioconjug. Chem. 17 (2006) 291–299.
[68] H.-F. Liang, C.-T. Chen, C. Sung-Ching, A.R. Kulkarni, Y.-L. Chiu, M.-C. Chen, H.-W. Sung, Paclitaxel-loaded poly(gamma-glutamic acid)-poly(lactide) nanoparticles as a targeted drug delivery system for the treatment of liver cancer, Biomaterials 27 (2006) 2051–2059.
[69] S.-N. Wang, Y.-H. Deng, H. Xu, H.-B. Wu, Y.-K. Qiu, D.-W. Chen, Synthesis of a novel galactosylated lipid and its application to the hepatocyte-selective targeting of liposomal doxorubicin, Eur. J. Pharm. Biopharm. 62 (2006) 32–38.
[70] S.A. Guhagarkar, R.V. Gaikwad, A. Samad, V.C. Malshe, P.V. Devarajan, Polyethylene sebacate-doxorubicin nanoparticles for hepatic targeting, Int. J. Pharm. 401 (2010) 113–122.
[71] X.-R. Qi, W.-W. Yan, J. Shi, Hepatocytes targeting of cationic liposomes modified with soybean sterylglucoside and polyethylene glycol, World J. Gastroenterol. 11 (2005) 4947–4952.
[72] M. Cheng, X. Gao, Y. Wang, H. Chen, B. He, H. Xu, Y. Li, J. Han, Z. Zhang, Synthesis of glycyrrhetinic acid-modified chitosan 5-fluorouracil nanoparticles and its inhibition of liver cancer characteristics in vitro and in vivo, Mar. Drugs 11 (2013) 3517–3536.
[73] Q. Tian, X.-H. Wang, W. Wang, C.-N. Zhang, P. Wang, Z. Yuan, Self-assembly and liver targeting of sulfated chitosan nanoparticles functionalized with glycyrrhetinic acid, Nanomedicine 8 (2012) 870–879.
[74] L. Shi, C. Tang, C. Yin, Glycyrrhizin-modified O-carboxymethyl chitosan nanoparticles as drug vehicles targeting hepatocellular carcinoma, Biomaterials 33 (2012) 7594–7604.
[75] W. Huang, W. Wang, P. Wang, Q. Tian, C. Zhang, C. Wang, Z. Yuan, M. Liu, H. Wan, H. Tang, Glycyrrhetinic acid-modified poly(ethylene glycol)-b-poly(gamma-benzyl l-glutamate) micelles for liver targeting therapy, Acta Biomater. 6 (2010) 3927–3935.
[76] C. Zhang, W. Wang, T. Liu, Y. Wu, H. Guo, P. Wang, Q. Tian, Y. Wang, Z. Yuan, Doxorubicin-loaded glycyrrhetinic acid-modified alginate nanoparticles for liver tumor chemotherapy, Biomaterials 33 (2012) 2187–2196.
[77] H. Guo, Q. Lai, W. Wang, Y. Wu, C. Zhang, Y. Liu, Z. Yuan, Functional alginate nanoparticles for efficient intracellular release of doxorubicin and hepatoma carcinoma cell targeting therapy, Int. J. Pharm. 451 (2013) 1–11.
[78] S.-J. Cheong, C.-M. Lee, S.-L. Kim, H.-J. Jeong, E.-M. Kim, E.-H. Park, D.W. Kim, S.T. Lim, M.-H. Sohn, Superparamagnetic iron oxide nanoparticles-loaded chitosan-linoleic acid nanoparticles as an effective hepatocyte-targeted gene delivery system, Int. J. Pharm. 372 (2009) 169–176.
[79] K.J. Longmuir, S.M. Haynes, J.L. Baratta, N. Kasabwalla, R.T. Robertson, Liposomal delivery of doxorubicin to hepatocytes in vivo by targeting heparan sulfate, Int. J. Pharm. 382 (2009) 222–233.
[80] D.-Y. Gao, T.-T. Lin, Y.-C. Sung, Y.C. Liu, W.-H. Chiang, C.-C. Chang, J.-Y. Liu, Y. Chen, CXCR4-targeted lipid-coated PLGA nanoparticles deliver sorafenib and overcome acquired drug resistance in liver cancer, Biomaterials 67 (2015) 194–203.
[81] X. Zhang, Q. Zhang, Q. Peng, J. Zhou, L. Liao, X. Sun, L. Zhang, T. Gong, Hepatitis B virus preS1-derived lipopeptide functionalized liposomes for targeting of hepatic cells, Biomaterials 35 (2014) 6130–6141.
[82] M. Rui, W. Guo, Q. Ding, X. Wei, J. Xu, Y. Xu, Recombinant high-density lipoprotein nanoparticles containing gadolinium-labeled cholesterol for morphologic and functional magnetic resonance imaging of the liver, Int. J. Nanomedicine 7 (2012) 3751–3768.
[83] T. Skajaa, D.P. Cormode, P.A. Jarzyna, A. Delshad, C. Blachford, A. Barazza, E.A. Fisher, R.E. Gordon, Z.A. Fayad, W.J.M. Mulder, The biological properties of iron oxide core high-density lipoprotein in experimental atherosclerosis, Biomaterials 32 (2011) 206–213.
[84] S.I. Kim, D. Shin, T.H. Choi, J.C. Lee, G.-J. Cheon, K.-Y. Kim, M. Park, M. Kim, Systemic and specific delivery of small interfering RNAs to the liver mediated by apolipoprotein A-I, Mol. Ther. 15 (2007) 1145–1152.
[85] G. Renaud, R.L. Hamilton, R.J. Havel, Hepatic metabolism of colloidal gold-low-density lipoprotein complexes in the rat: evidence for bulk excretion of lysosomal contents into bile, Hepatology 9 (1989) 380–392.
[86] S.M. Moghimi, A.C. Hunter, J.C. Murray, Long-circulating and target-specific nanoparticles: theory to practice, Pharmacol. Rev. 53 (2001) 283–318.
[87] M. Longmire, P.L. Choyke, H. Kobayashi, Clearance properties of nano-sized particles and molecules as imaging agents: considerations and caveats, Nanomedicine 3 (2008) 703–717.
[88] C. He, Y. Hu, L. Yin, C. Tang, C. Yin, Effects of particle size and surface charge on cellular uptake and biodistribution of polymeric nanoparticles, Biomaterials 31 (2010) 3657–3666.
[89] K.-i. Ogawara, M. Yoshida, K. Higaki, T. Kimura, K. Shiraishi, M. Nishikawa, Y. Takakura, M. Hashida, Hepatic uptake of polystyrene microshperes in rats: effect of particle size on intrahepatic distribution, J. Control. Release 59 (1999) 15–22.
[90] Y. Takakura, R.I. Mahato, M. Hashida, Extravasation of macromolecules, Adv. Drug Deliv. Rev. 34 (1998) 93–108.
[91] M. Gaumet, A. Vargas, R. Gurny, F. Delie, Nanoparticles for drug delivery: the need for precision in reporting particle size parameters, Eur. J. Pharm. Biopharm. 69 (2008) 1–9.
[92] K. Poelstra, J. Prakash, L. Beljaars, Drug targeting to the diseased liver, J. Control. Release 161 (2012) 188–197.
[93] M. Bartsch, D.K.F. Meijer, A.H. Weeke-Klimp, G.L. Scherphof, J.A.A.M. Kamps, Massive and selective delivery of lipid-coated cationic lipoplexes of oligonucleotides targeted in vivo to hepatic endothelial cells, Pharm. Res. 19 (2002).
[94] P. Chevallier, A. Walter, A. Garofalo, I. Veksler, J. Lagueux, S. Bégin-Colin, D. Felder-Flesch, M.-A. Fortin, Tailored biological retention and efficient clearance of pegylated ultra-small MnO nanoparticles as positive MRI contrast agents for molecular imaging, J. Mater. Chem. B 2 (2014) 1779.
[95] L. Yang, Y.-C. Lee, M.I. Kim, H.G. Park, Y.S. Huh, Y. Shao, H.-K. Han, Biodistribution and clearance of aminoclay nanoparticles: implication for in vivo applicability as a tailor-made drug delivery carrier, J. Mater. Chem. B 2 (2014) 7567–7574.
[96] Z. Chen, H. Chen, H. Meng, G. Xing, X. Gao, B. Sun, X. Shi, H. Yuan, C. Zhang, R. Liu, F. Zhao, Y. Zhao, X. Fang, Bio-distribution and metabolic paths of silica coated CdSeS quantum dots, Toxicol. Appl. Pharmacol. 230 (2008) 364–371.
[97] P. Bourrinet, H.H. Bengele, B. Bonnemain, A. Dencausse, J.-M. Idee, P.M. Jacobs, J.M. Lewis, Preclinical safety and pharmacokinetic profile of ferumoxtran-10, an ultrasmall superparamagnetic iron oxide magnetic resonance contrast agent, Investig. Radiol. 41 (2006) 313–324.
[98] R. Kumar, I. Roy, T.Y. Ohulchanskky, L.A. Vathy, E.J. Bergey, M. Sajjad, P.N. Prasad, In vivo biodistribution and clearance studies using multimodal organically modified silica nanoparticles, ACS Nano 4 (2010) 699–708.
[99] J. Lu, M. Liong, Z. Li, J.I. Zink, F. Tamanoi, Biocompatibility, biodistribution, and drug-delivery efficiency of mesoporous silica nanoparticles for cancer therapy in animals, Small 6 (2010) 1794–1805.
[100] S. Ye, G. Marston, J.R. McLaughlan, D.O. Sigle, N. Ingram, S. Freear, J.J. Baumberg, R.J. Bushby, A.F. Markham, K. Critchley, P.L. Coletta, S.D. Evans, Engineering gold nanotubes with controlled length and near-infrared absorption for theranostic applications, Adv. Funct. Mater. 25 (2015) 2117–2127.
[101] M. Semmler-Behnke, W.G. Kreyling, J. Lipka, S. Fertsch, A. Wenk, S. Takenaka, G. Schmid, W. Brandau, Biodistribution of 1.4- and 18-nm gold particles in rats, Small 4 (2008) 2108–2111.
[102] S. Hirn, M. Semmler-Behnke, C. Schleh, A. Wenk, J. Lipka, M. Schäffler, S. Takenaka, W. Möller, G. Schmid, U. Simon, W.G. Kreyling, Particle size-dependent and surface charge-dependent biodistribution of gold nanoparticles after intravenous administration, Eur. J. Pharm. Biopharm. 77 (2011) 407–416.
[103] L. Wang, Y.-F. Li, L. Zhou, Y. Liu, L. Meng, K. Zhang, X. Wu, L. Zhang, B. Li, C. Chen, Characterization of gold nanorods in vivo by integrated analytical techniques: their uptake, retention, and chemical forms, Anal. Bioanal. Chem. 396 (2010) 1105–1114.
[104] E. Sadauskas, G. Danscher, M. Stoltenberg, U. Vogel, A. Larsen, H. Wallin, Protracted elimination of gold nanoparticles from mouse liver, Nanomedicine 5 (2009) 162–169.
[105] S.K. Balasubramanian, J. Jittiwat, J. Manikandan, C.-N. Ong, L.E. Yu, W.-Y. Ong, Biodistribution of gold nanoparticles and gene expression changes in the liver and spleen after intravenous administration in rats, Biomaterials 31 (2010) 2034–2042.
[106] T.K. Jain, M.K. Reddy, M.A. Morales, D.L. Leslie-Pelecky, V. Labhasetwar, Biodistribution, clearance, and biocompatibility of iron oxide magnetic nanoparticles in rats, Mol. Pharm. 5 (2008) 316–327.
[107] E.A. Sykes, Q. Dai, K.M. Tsoi, D.M. Hwang, W.C.W. Chan, Nanoparticle exposure in animals can be visualized in the skin and analysed via skin biopsy, Nat. Commun. 5 (2014) 3796.
[108] X. Huang, L. Li, T. Liu, N. Hao, H. Liu, D. Chen, F. Tang, The shape effect of mesoporous silica nanoparticles on biodistribution, clearance, and biocompatibility in vivo, ACS Nano 5 (2011) 5390–5399.
[109] M. Cho, W.-S. Cho, M. Choi, S.J. Kim, B.S. Han, S.H. Kim, H.O. Kim, Y.Y. Sheen, J. Jeong, The impact of size on tissue distribution and elimination by single intravenous injection of silica nanoparticles, Toxicol. Lett. 189 (2009) 177–183.
[110] J.S. Souris, C.-H. Lee, S.-H. Cheng, C.-T. Chen, C.-S. Yang, J.-a.A. Ho, C.-Y. Mou, L.-W. Lo, Surface charge-mediated rapid hepatobiliary excretion of mesoporous silica nanoparticles, Biomaterials 31 (2010) 5564–5574.
[111] C. Fu, T. Liu, L. Li, H. Liu, D. Chen, F. Tang, The absorption, distribution, excretion and toxicity of mesoporous silica nanoparticles in mice following different exposure routes, Biomaterials 34 (2013) 2565–2575.
[112] T. Yu, D. Hubbard, A. Ray, H. Ghandehari, In vivo biodistribution and pharmacokinetics of silica nanoparticles as a function of geometry, porosity and surface characteristics, J. Control. Release 163 (2012) 46–54.
[113] J.W.M. Bulte, A.H. Schmieder, J. Keupp, S.D. Caruthers, S.A. Wickline, G.M. Lanza, MR cholangiography demonstrates unsuspected rapid biliary clearance of nanoparticles in rodents: implications for clinical translation, Nanomedicine 10 (2014) 1385–1388.
[114] J. Lipka, M. Semmler-Behnke, R.A. Sperling, A. Wenk, S. Takenaka, C. Schleh, T. Kissel, W.J. Parak, W.G. Kreyling, Biodistribution of PEG-modified gold nanoparticles following intratracheal instillation and intravenous injection, Biomaterials 31 (2010) 6574–6581.
[115] J. Xiao, X.M. Tian, C. Yang, P. Liu, N.Q. Luo, Y. Liang, H.B. Li, D.H. Chen, C.X. Wang, L. Li, G.W. Yang, Ultrahigh relaxivity and safe probes of manganese oxide nanoparticles for in vivo imaging, Sci. Rep. 3 (2013).
[116] K. Park, E.-J. Park, I.K. Chun, K. Choi, S.H. Lee, J. Yoon, B.C. Lee, Bioavailability and toxicokinetics of citrate-coated silver nanoparticles in rats, Arch. Pharm. Res. 34 (2011) 153–158.
[117] C.Y. Watson, R.M. Molina, A. Louzada, K.M. Murdaugh, T.C. Donaghey, J.D. Brain, Effects of zinc oxide nanoparticles on Kupffer cell phagosomal motility, bacterial clearance, and liver function, Int. J. Nanomedicine 10 (2015) 4173–4184.
[118] C. Liu, Z. Gao, J. Zeng, Y. Hou, F. Fang, Y. Li, R. Qiao, L. Shen, H. Lei, W. Yang, M. Gao, Magnetic/upconversion fluorescent NaGdF4:Yb,Er nanoparticle-based

dual-modal molecular probes for imaging tiny tumors in vivo, ACS Nano 7 (2013) 7227–7240.
[119] Z. Amoozgar, Y. Yeo, Recent advances in stealth coating of nanoparticle drug delivery systems, Wiley Interdiscip. Rev. Nanomed. Nanobiotechnol. 4 (2012) 219–233.
[120] P.P. Karmali, D. Simberg, Interactions of nanoparticles with plasma proteins: implication on clearance and toxicity of drug delivery systems, Expert Opin. Drug Deliv. 8 (2011) 343–357.
[121] N. Desai, Challenges in development of nanoparticle-based therapeutics, AAPS J. 14 (2012) 282–295.
[122] H.S. Choi, W. Liu, P. Misra, E. Tanaka, J.P. Zimmer, B. Itty Ipe, M.G. Bawendi, J.V. Frangioni, Renal clearance of quantum dots, Nat. Biotechnol. 25 (2007) 1165–1170.
[123] M. Elsabahy, K.L. Wooley, Design of polymeric nanoparticles for biomedical delivery applications, Chem. Soc. Rev. 41 (2012) 2545–2561.
[124] L.M. Lacava, V. Garcia, S. Kuchelhaus, R.B. Azevedo, N. Sadeghiani, N. Buske, P.C. Morais, Z.G.M. Lacava, Long-term retention of dextran-coated magnetite nanoparticles in the liver and spleen, J. Magn. Magn. Mater. 272–276 (2004) 2434–2435.
[125] J. Kolosnjaj-Tabi, Y. Javed, L. Lartigue, J. Volatron, D. Elgrabli, I. Marangon, G. Pugliese, B. Caron, A. Figuerola, N. Luciani, T. Pellegrino, D. Alloyeau, F. Gazeau, The one year fate of iron oxide coated gold nanoparticles in mice, ACS Nano 9 (2015) 7925–7939.
[126] Y. Pan, S. Neuss, A. Leifert, M. Fischler, F. Wen, U. Simon, G. Schmid, W. Brandau, W. Jahnen-Dechent, Size-dependent cytotoxicity of gold nanoparticles, Small 3 (2007) 1941–1949.
[127] T. Xia, M. Kovochich, M. Liong, L. Mädler, B. Gilbert, H. Shi, J.I. Yeh, J.I. Zink, A.E. Nel, Comparison of the mechanism of toxicity of zinc oxide and cerium oxide nanoparticles based on dissolution and oxidative stress properties, ACS Nano 2 (2008) 2121–2134.
[128] S. George, S. Pokhrel, T. Xia, B. Gilbert, Z. Ji, M. Schowalter, A. Rosenauer, R. Damoiseaux, K.A. Bradley, L. Mädler, A.E. Nel, Use of a rapid cytotoxicity screening approach to engineer a safer zinc oxide nanoparticle through iron doping, ACS Nano 4 (2010) 15–29.
[129] H.-J. Paek, Y.-J. Lee, H.-E. Chung, N.-H. Yoo, J.-A. Lee, M.-K. Kim, J.K. Lee, J. Jeong, S.-J. Choi, Modulation of the pharmacokinetics of zinc oxide nanoparticles and their fates in vivo, Nanoscale 5 (2013) 11416–11427.
[130] N.F. Krebs, K.M. Hambidge, Zinc metabolism and homeostasis: the application of tracer techniques to human zinc physiology, Biometals 14 (2001) 397–412.
[131] E.J. Martinez-Finley, S. Chakraborty, F. J.B., M. Aschner, Cellular transport and homeostasis of essential and nonessential metals, Metallomics 4 (2012) 593–605.
[132] V. Hower, P. Mendes, F.M. Torti, R. Laubenbacher, S. Akman, V. Shulaev, S.V. Torti, A general map of iron metabolism and tissue-specific subnetworks, Mol. BioSyst. 5 (2009) 422–443.
[133] G. Papanikolaou, K. Pantopoulos, Iron metabolism and toxicity, Toxicol. Appl. Pharmacol. 202 (2005) 199–211.
[134] K. Briley-Saebo, H. Ahlstrom, A. Bjørnerud, T. Berg, D. Grant, G.M. Kindberg, Hepatic cellular distribution and degradation of iron oxide nanoparticles following single intravenous injection in rats: implications for magnetic resonance imaging, Cell Tissue Res. 316 (2004) 315–323.
[135] M. Levy, N. Luciani, D. Alloyeau, D. Elgrabli, V. Deveaux, C. Pechoux, S. Chat, G. Wang, N. Vats, F. Gendron, C. Factor, S. Lotersztajn, A. Luciani, C. Wilhelm, F. Gazeau, Long term in vivo biotransformation of iron oxide nanoparticles, Biomaterials 32 (2011) 3988–3999.
[136] E.J. King, M. Mcgeorge, The biochemistry of silicic acid, Biochem. J. 32 (1938) 426–433.
[137] Q. He, Z. Zhang, Y. Gao, J. Shi, Y. Li, Intracellular localization and cytotoxicity of spherical mesoporous silica nano- and microparticles, Small 5 (2009) 2722–2729.
[138] J.-H. Park, L. Gu, G. von Maltzahn, E. Ruoslahti, S.N. Bhatia, M.J. Sailor, Biodegradable luminescent porous silicon nanoparticles for in vivo applications, Nat. Mater. 8 (2009) 331–336.
[139] X. He, H. Nie, K. Wang, W. Tan, X. Wu, P. Zhang, In vivo study of biodistribution and urinary excretion of surface-modified silica nanoparticles, Anal. Chem. 80 (2008) 9597–9603.
[140] F. Chen, S. Goel, H.F. Valdovinos, H. Luo, R. Hernandez, T.E. Barnhart, W. Cai, In vivo integrity and biological fate of chelator-free zirconium-89-labeled mesoporous silica nanoparticles, ACS Nano 9 (2015) 7950–7959.
[141] A.A. D'Souza, P.V. Devarajan, Asialoglycoprotein receptor mediated hepatocyte targeting — strategies and applications, J. Control. Release 203 (2015) 126–139.
[142] J.M. Bergen, H.A. von Recum, T.T. Goodman, A.P. Massey, S.H. Pun, Gold nanoparticles as a versatile platform for optimizing physicochemical parameters for targeted drug delivery, Macromol. Biosci. 6 (2006) 506–516.
[143] T. Yamada, Y. Iwasaki, H. Tada, H. Iwabuki, M.K. Chuah, T. VandenDriessche, H. Fukuda, A. Kondo, M. Ueda, M. Seno, K. Tanizawa, S. Kuroda, Nanoparticles for the delivery of genes and drugs to human hepatocytes, Nat. Biotechnol. 21 (2003) 885–890.
[144] S.-H. Cheng, F.-C. Li, J.S. Souris, C.-S. Yang, F.-G. Tseng, H.-S. Lee, C.-T. Chen, C.-Y. Dong, L.-W. Lo, Visualizing dynamics of sub-hepatic distribution of nanoparticles using intravital multiphoton fluorescence microscopy, ACS Nano 6 (2012) 4122–4131.
[145] D. Eberle, R. Clarke, N. Kaplowitz, Rapid oxidation in vitro of endogenous and exogenous glutathione in bile of rats, J. Biol. Chem. 256 (1980) 2115–2117.
[146] O.B. Ijare, B.S. Somashekar, G.A.N. Gowda, A. Sharma, V.K. Kapoor, C.L. Khetrapal, Quantification of glycine and taurine conjugated bile acids in human bile using ^{1}H NMR spectroscopy, Magn. Reson. Med. 53 (2005) 1441–1446.
[147] A. Walter, A. Garofalo, A. Parat, J. Jouhannaud, G. Pourroy, E. Voirin, S. Laurent, P. Bonazza, J. Taleb, C. Billotey, L. Vander Elst, R.N. Muller, S. Begin-Colin, D. Felder-Flesch, Validation of a dendron concept to tune colloidal stability, MRI relaxivity and bioelimination of functional nanoparticles, J. Mater. Chem. B 3 (2015) 1484–1494.
[148] G. Lamanna, M. Kueny-Stotz, H. Mamlouk-Chaouachi, C. Ghobril, B. Basly, A. Bertin, I. Miladi, C. Billotey, G. Pourroy, S. Begin-Colin, D. Felder-Flesch, Dendronized iron oxide nanoparticles for multimodal imaging, Biomaterials 32 (2011) 8562–8573.
[149] C.-J. Lin, N. Kang, J.-Y. Lee, H.-S. Lee, C.-Y. Dong, Visualizing and quantifying difference in cytoplasmic and nuclear metabolism in the hepatobiliary system in vivo, J. Biomed. Opt. 20 (2015) 16020.
[150] Y. Geng, P. Dalhaimer, S. Cai, R. Tsai, M. Tewari, T. Minko, D.E. Discher, Shape effects of filaments versus spherical particles in flow and drug delivery, Nat. Nanotechnol. 2 (2007) 249–255.
[151] S.-Y. Lin, W.-H. Hsu, J.-M. Lo, H.-C. Tsai, G.-H. Hsiue, Novel geometry type of nanocarriers mitigated the phagocytosis for drug delivery, J. Control. Release 154 (2011) 84–92.
[152] M.M. Arnida, A. Janát-Amsbury, C.M. Ray, H. Peterson, Ghandehari, geometry and surface characteristics of gold nanoparticles influence their biodistribution and uptake by macrophages, Eur. J. Pharm. Biopharm. 77 (2011) 417–423.
[153] P. Decuzzi, B. Godin, T. Tanaka, S.-Y. Lee, C. Chiappini, X. Liu, M. Ferrari, Size and shape effects in the biodistribution of intravascularly injected particles, J. Control. Release 141 (2010) 320–327.
[154] J.A. Champion, S. Mitragotri, Shape induced inhibition of phagocytosis of polymer particles, Pharm. Res. 26 (2009) 244–249.
[155] A. Musyanovych, J. Dausend, M. Dass, P. Walther, V. Mailänder, K. Landfester, Criteria impacting the cellular uptake of nanoparticles: a study emphasizing polymer type and surfactant effects, Acta Biomater. 7 (2011) 4160–4168.
[156] K.A. Beningo, Y.-L. Wang, Fc-receptor-mediated phagocytosis is regulated by mechanical properties of the target, J. Cell Sci. 115 (2002) 849–856.
[157] T.J. Merkel, S.W. Jones, K.P. Herlihy, F.R. Kersey, A.R. Shields, M. Napier, J.C. Luft, H. Wu, W.C. Zamboni, A.Z. Wang, J.E. Bear, J.M. DeSimone, Using mechanobiological mimicry of red blood cells to extend circulation times of hydrogel microparticles, Proc. Natl. Acad. Sci. U. S. A. 108 (2011) 586–591.
[158] A.A. Gabizon, Liposome circulation time and tumor targeting: implications for cancer chemotherapy, Adv. Drug Deliv. Rev. 16 (1995) 285–294.
[159] Q. Dai, C. Walkey, W.C.W. Chan, Polyethylene glycol backfilling mitigates the negative impact of the protein corona on nanoparticle cell targeting, Angew. Chem. Int. Ed. 53 (2014) 5093–5096.
[160] M. Bartneck, H.A. Keul, S. Singh, K. Czaja, J. Bornemann, M. Bockstaller, M. Moeller, G. Zwadlo-Klarwasser, J. Groll, Rapid uptake of gold nanorods by primary human blood phagocytes and immunomodulatory effects of surface chemistry, ACS Nano 4 (2010) 3073–3086.
[161] A.J. Keefe, S. Jiang, Poly(zwitterionic)protein conjugates offer increased stability without sacrificing binding affinity or bioactivity, Nat. Chem. 4 (2012) 59–63.
[162] J.B. Schlenoff, Zwitteration: coating surfaces with zwitterionic functionality to reduce nonspecific adsorption, Langmuir 30 (2014) 9625–9636.
[163] S. Jiang, Z. Cao, Ultralow-fouling, functionalizable, and hydrolyzable zwitterionic materials and their derivatives for biological applications, Adv. Mater. 22 (2010) 920–932.
[164] T. Liu, H. Choi, R. Zhou, I.-W. Chen, RES blockade: a strategy for boosting efficiency of nanoparticle drug, Nano Today 10 (2015) 11–21.
[165] V.P. Torchilin, Recent advances with liposomes as pharmaceutical carriers, Nat. Rev. Drug Discov. 4 (2005) 145–160.
[166] N. van Rooijen, A. Sanders, Liposome mediated depletion of macrophage, mechanism of action, preparation of liposomes and applications, J. Immunol. Methods 174 (1994) 83–93.
[167] N. van Rooijen, Liposomes for targeting of antigens and drugs: immunoadjuvant activity and liposome-mediated depletion of macrophages, J. Drug Target. 16 (2008) 529–534.
[168] P.P. Lehenkari, M. Kellinsalmi, J.P. Näpänkangas, K.V. Ylitalo, J. Mönkkönen, M.J. Rogers, A. Azhayev, H.K. Väänänen, I.E. Hassinen, Further insight into mechanism of action of clodronate: inhibition of mitochondrial ADP/ATP translocase by a nonhydrolyzable, adenine-containing metabolite, Mol. Pharmacol. 62 (2002) 1255–1262.
[169] A.C. Kirby, L. Beattie, A. Maroof, N. van Rooijen, P.M. Kaye, SIGNR1-negative red pulp macrophages protect against acute streptococcal sepsis after *Leishmania donovani*-induced loss of marginal zone macrophages, Am. J. Pathol. 175 (2009) 1107–1115.
[170] Q. Hu, N. van Rooijen, D. Liu, Effect of macrophage elimination using liposome-encapsulated dichloromethylene diphosphonate on tissue distribution of liposomes, J. Lipid Res. 6 (1996) 681–698.
[171] Y. Ohara, T. Oda, K. Yamada, S. Hashimoto, Y. Akashi, R. Miyamoto, A. Kobayashi, K. Fukunaga, R. Sasaki, N. Ohkohchi, Effective delivery of chemotherapeutic nanoparticles by depleting host Kupffer cells, Int. J. Cancer 131 (2012) 2402–2410.
[172] D. Simberg, T. Duza, J.H. Park, M. Essler, J. Pilch, L. Zhang, A.M. Derfus, M. Yang, R.M. Hoffman, S. Bhatia, M.J. Sailor, E. Ruoslahti, Biomimetic amplification of nanoparticle homing to tumors, Proc. Natl. Acad. Sci. U. S. A. 104 (2007) 932–936.
[173] S.J. Kennel, J.D. Woodward, A.J. Rondinone, J. Wall, Y. Huang, S. Mirzadeh, The fate of MAb-targeted Cd^{125m}Te/ZnS nanoparticles in vivo, Nucl. Med. Biol. 35 (2008) 501–514.
[174] D. Ruttinger, B. Vollmar, G.A. Wanner, K. Messmer, In vivo assessment of hepatic alterations following gadolinium chloride-induced Kupffer cell blockade, J. Hepatol. 25 (1996) 960–967.

[175] E. Husztik, G. Lazar, A. Parducz, Electron microscopic study of Kupffer-cell phagocytosis blockade induced by gadolinium chloride, Br. J. Exp. Pathol. 61 (1980) 624–630.
[176] M.J. Hardonk, F. Dijkhuis, C.E. Hulstaert, J. Koudstaal, Heterogeneity of rat liver and spleen macrophages in Gadolinium chloride-induced elimination and repopulation, J. Leukoc. Biol. 52 (1992) 296–302.
[177] P. Diagaradjane, A. Deorukhkar, J.G. Gelovani, D.M. Maru, S. Krishnan, Gadolinium chloride augments tumor-specific imaging of targeted quantum dots in vivo, ACS Nano 4 (2010) 4131–4141.
[178] J.-W. Yoo, D.J. Irvine, D.E. Discher, S. Mitragotri, Bio-inspired, bioengineered and biomimetic drug delivery carriers, Nat. Rev. Drug Discov. 10 (2011) 521–535.
[179] A.C. Anselmo, V. Gupta, B.J. Zern, D. Pan, M. Zakrewsky, V. Muzykantov, S. Mitragotri, Delivering nanoparticles to lungs while avoiding liver and spleen through adsorption on red blood cells, ACS Nano 7 (2013) 11129–11137.
[180] A. Parodi, N. Quattrocchi, A.L. van de Ven, C. Chiappini, M. Evangelopoulos, J.O. Martinez, B.S. Brown, S.Z. Khaled, I.K. Yazdi, M.V. Enzo, L. Isenhart, M. Ferrari, E. Tasciotti, Synthetic nanoparticles functionalized with biomimetic leukocyte membranes possess cell-like functions, Nat. Nanotechnol. 8 (2013) 61–68.
[181] M.-R. Choi, K.J. Stanton-Maxey, J.K. Stanley, C.S. Levin, R. Bardhan, D. Akin, S. Badve, J. Sturgis, J.P. Robinson, R. Bashir, N.J. Halas, S.E. Clare, A cellular Trojan Horse for delivery of therapeutic nanoparticles into tumors, Nano Lett. 7 (2007) 3759–3765.
[182] J. Choi, H.-Y. Kim, E.J. Ju, J. Jung, J. Park, H.-K. Chung, J.S. Lee, J.S. Lee, H.J. Park, S.Y. Song, S.-Y. Jeong, E.K. Choi, Use of macrophages to deliver therapeutic and imaging contrast agents to tumors, Biomaterials 33 (2012) 4195–4203.
[183] N. Doshi, A.S. Zahr, S. Bhaskar, J. Lahann, S. Mitragotri, Red blood cell-mimicking synthetic biomaterial particles, Proc. Natl. Acad. Sci. U. S. A. 106 (2009) 21495–21499.
[184] C.-M.J. Hu, R.H. Fang, J. Copp, B.T. Luk, L. Zhang, A biomimetic nanosponge that absorbs pore-forming toxins, Nat. Nanotechnol. 8 (2013) 336–340.